CD –24°17504 REVISITED: A NEW COMPREHENSIVE ELEMENT ABUNDANCE ANALYSIS

Citation: Jacobson, Heather R., and Anna Frebel. "CD –24°17504 REVISITED: A NEW COMPREHENSIVE ELEMENT ABUNDANCE ANALYSIS." The Astrophysical Journal 808, no. 1 (July 17, 2015): 53. © 2015 The American Astronomical Society

As Published: http://dx.doi.org/10.1088/0004-637x/808/1/53

Publisher: IOP Publishing

Persistent URL: http://hdl.handle.net/1721.1/99906

Version: Final published version: final published article, as it appeared in a journal, conference proceedings, or other formally published context

The Astrophysical Journal, 808:53 (21pp), 2015 July 20 doi:10.1088/0004-637X/808/1/53

CD −24°17504 REVISITED: A NEW COMPREHENSIVE ELEMENT ABUNDANCE ANALYSIS*

Heather R. Jacobson and Anna Frebel
Kavli Institute for Astrophysics and Space Research and Department of Physics, Massachusetts Institute of Technology, 77 Massachusetts Avenue, Cambridge, MA 02139, USA
Received 2015 February 13; accepted 2015 June 15; published 2015 July 17

ABSTRACT

With [Fe/H] ∼ −3.3, CD −24°17504 is a canonical metal-poor main-sequence turn-off star. Though it has appeared in numerous literature studies, the most comprehensive abundance analysis for the star based on high-resolution, high signal-to-noise ratio (S/N) spectra is nearly 15 years old. We present a new detailed abundance analysis for 21 elements based on combined archival Keck-HIRES and Very Large Telescope-UVES spectra of the star that is higher in both spectral resolution and S/N than previous data. Our results are very similar to those of an earlier comprehensive study of the star, but we present for the first time a carbon abundance from the CH G-band feature as well as improved upper limits for neutron-capture species such as Y, Ba, and Eu. In particular, we find that CD −24°17504 has [Fe/H] = −3.41, [C/Fe] = +1.10, [Sr/H] = −4.68, and [Ba/H] ⩽ −4.46, making it a carbon-enhanced metal-poor star with neutron-capture element abundances among the lowest measured in Milky Way halo stars.

Key words: stars: abundances – stars: fundamental parameters – stars: Population II

1. INTRODUCTION

Metal-poor stars, especially those with [Fe/H] $\lesssim$ −3, are highly sought after because of the information they provide about early generations of star formation and chemical evolution in the universe. The number of stars known to have [Fe/H] $\lesssim$ −3 has greatly expanded in recent years due to dedicated searches for such objects and now is of the order of 10^3 (Beers et al. 1992; Cayrel et al. 2004; Christlieb et al. 2008; Lai et al. 2008; Caffau et al. 2011; Aoki et al. 2013; Cohen et al. 2013; Norris et al. 2013; Roederer et al. 2014; Frebel & Norris 2015).

With a visual magnitude bright enough ($V \sim 12$) to place it in the 1892 Cordoba Durchmusterung (CD; Thome 1892) catalog, CD −24°17504 also appeared in catalogs of high proper motion stars, such as the New Luyten catalog of Stars with Proper Motions Larger than Two Tenths of an arcsecond (NLTT; Luyten 1980). In a survey for subdwarfs, Ryan (1989) found it in the NLTT catalog, and follow-up spectroscopic studies at low and high resolution showed it to be extremely metal-poor (Ryan et al. 1991; Ryan & Norris 1991). The first high-resolution spectroscopic study of this star was done by Ryan et al. (1991), and this study was superceded by a work with better data in Norris et al. (2001). It remains one of the most well-studied extremely metal-poor turn-off stars to this day, due its bright visual magnitude. In addition to the comprehensive element abundances presented by Norris et al., the abundances of light elements (Primas et al. 2000; Meléndez & Ramírez 2004; Aoki et al. 2009; Fabbian et al. 2009; Hosford et al. 2009; Rich & Boesgaard 2009), α-elements (Israelian et al. 2001; Arnone et al. 2005; Fabbian et al. 2009; Ishigaki et al. 2012), and Fe-peak elements (Bihain et al. 2004; Nissen et al. 2007; Ishigaki et al. 2013) in CD −24°17504 have been studied in some detail by several different authors.

Given the relatively high effective temperatures and surface gravities of metal-poor stars near the main-sequence turn-off (MSTO), their spectra can contain few absorption features suitable for detailed high resolution spectroscopic study. Although CD −24°17504 is one of the brightest metal-poor dwarf stars known, only upper limits for the neutron-capture species Ba and Eu can be determined. Because CD −24° 17504 is a canonical metal-poor star, it is worthwhile to beat down the upper limits to some abundance measurements to better constrain its nucleosynthetic origin. Spectra of resolution and signal-to-noise ratio (S/N) superior to that used by Norris et al. (2001) (hereafter NRB01) have since been obtained for CD −24°17504. Of these, only Ishigaki et al. (2010, 2012, 2013) have presented abundances for selected α-, Fe-peak, and neutron-capture species for CD −24°17504 as part of their comprehensive study of stars in the outer Milky Way halo.[1] However, their analyses included only a few lines per species, and do not include an evaluation of C, Li or neutron-capture species beyond Sr and Eu.

Therefore, we consider it time to revisit CD −24°17504 in its own right, separate from any large sample studies and in order to obtain as much abundance information as possible from the best available data. We have searched archival databases for spectra of CD −24°17504 and present here the results of a comprehensive detailed abundance analysis, with emphasis on elements previously undetected in CD −24°17504 and those with upper limits. We describe the data in Section 2, the methods of our analysis in Section 3, and the results in Section 4. A summary and conclusions are given in Section 5.

2. ARCHIVAL SPECTRA

The data used in this work are high-resolution spectra from the ESO and Keck archive facilities. Details of the individual exposures are given in Table 1 for all the data used in this

* This work is based on data obtained from the ESO Science Archive Facility and associated with Programs 68.D-0094(A) and 073.D-0024(A). This work is also based on data obtained from the Keck Observatory Archive (KOA), which is operated by the W.M. Keck Obsevatory and the NASA Exoplanet Science Institute (NExScI), under contract with the National Aeronautics and Space Administration. These data are associated with Program C01H (P.I. Mélendez).

[1] We note that Yong et al. (2013a) presented a comprehensive abundance analysis of CD −24°17504; however, their analysis used the equivalent widths (EWs) of NRB01, and therefore can be considered an "update" of that work in an effort to place it on a homogeneous scale with their larger sample.

Table 1
Details of Archival Spectra of CD −24°17504 Used in this Work

Filename	Instrument	λ (Å)	$R \equiv \lambda/\Delta\lambda$	S/N[a]@ 4500 Å	S/N[a]@ 6000 Å	Exp Time (s)	P.I.	Prop ID / References[b]	UT Date
ADP.2013-09-25T06:40:48.133.fits	UVES	4780–6800	51,700	…	24	101	Primas	68.D-0094(A)	2001 Nov 26
ADP.2013-09-25T06:40:48.143.fits	UVES	4780–6800	51,700	…	100	1000	Primas	68.D-0094(A)	2001 Nov 26
ADP.2013-09-25T06:40:48.237.fits	UVES	4780–6800	51,700	…	118	1000	Primas	68.D-0094(A)	2001 Nov 26
ADP.2013-09-25T06:40:48.420.fits	UVES	4780–6800	51,700	…	128	1000	Primas	68.D-0094(A)	2001 Nov 26
ADP.2013-09-25T06:40:48.520.fits	UVES	4780–6800	51,700	…	196	1000	Primas	68.D-0094(A)	2001 Nov 26
ADP.2013-09-25T06:46:55.763.fits	UVES	4780–6800	51,700	…	146	1000	Primas	68.D-0094(A)	2001 Nov 27
ADP.2013-09-25T06:46:55.890.fits	UVES	4780–6800	51,700	…	156	1000	Primas	68.D-0094(A)	2001 Nov 27
ADP.2013-09-25T06:46:55.930.fits	UVES	4780–6800	51,700	…	138	1000	Primas	68.D-0094(A)	2001 Nov 27
ADP.2013-09-26T07:38:05.573.fits	UVES	3750–4970	53,000	75	…	975	Akerman	073.D-0024(A)	2004 Aug 07
ADP.2013-09-26T07:38:05.580.fits	UVES	3750–4970	53,000	87	…	975	Akerman	073.D-0024(A)	2004 Aug 07
ADP.2013-09-26T07:38:05.607.fits	UVES	3750–4970	53,000	59	…	975	Akerman	073.D-0024(A)	2004 Aug 07
ADP.2013-09-26T07:38:05.620.fits	UVES	3750–4970	53,000	96	…	975	Akerman	073.D-0024(A)	2004 Aug 08
ADP.2013-09-26T07:38:05.627.fits	UVES	3750–4970	53,000	69	…	975	Akerman	073.D-0024(A)	2004 Aug 07
ADP.2013-09-26T07:38:05.653.fits	UVES	3750–4970	53,000	69	…	975	Akerman	073.D-0024(A)	2004 Aug 07
ADP.2013-09-26T07:38:05.693.fits	UVES	3750–4970	53,000	115	…	975	Akerman	073.D-0024(A)	2004 Aug 07
ADP.2013-09-26T07:38:05.753.fits	UVES	3750–4970	53,000	74	…	975	Akerman	073.D-0024(A)	2004 Aug 07
ADP.2013-09-26T07:40:12.363.fits	UVES	3750–4970	53,000	87	…	975	Akerman	073.D-0024(A)	2004 Aug 10
ADP.2013-09-26T07:40:12.450.fits	UVES	3750–4970	53,000	61	…	975	Akerman	073.D-0024(A)	2004 Aug 10
ADP.2013-09-26T07:40:12.470.fits	UVES	3750–4970	53,000	94	…	975	Akerman	073.D-0024(A)	2004 Aug 10
ADP.2013-09-26T07:40:12.477.fits	UVES	3750–4970	53,000	72	…	975	Akerman	073.D-0024(A)	2004 Aug 10
ADP.2013-09-26T07:40:12.510.fits	UVES	3750–4970	53,000	68	…	975	Akerman	073.D-0024(A)	2004 Aug 10
ADP.2013-09-26T07:40:12.523.fits	UVES	3750–4970	53,000	65	…	975	Akerman	073.D-0024(A)	2004 Aug 10
ADP.2013-09-26T07:40:12.563.fits	UVES	3750–4970	53,000	78	…	975	Akerman	073.D-0024(A)	2004 Aug 10
ADP.2013-09-26T07:55:28.080.fits	UVES	3750–4970	53,000	61	…	975	Akerman	073.D-0024(A)	2004 Sep 01
ADP.2013-09-26T07:55:28.217.fits	UVES	3750–4970	53,000	65	…	975	Akerman	073.D-0024(A)	2004 Sep 01
ADP.2013-09-26T07:55:28.230.fits	UVES	3750–4970	53,000	114	…	975	Akerman	073.D-0024(A)	2004 Sep 01
HI.20050617.48772.fits	HIRES	3930–6895	103,000	106	197	1200	Mélendez	C01H	2005 Jul 17
HI.20050617.50045.fits	HIRES	3930–6895	103,000	103	179	1200	Mélendez	C01H	2005 Jul 17
HI.20050617.51319.fits	HIRES	3930–6895	103,000	108	164	1200	Mélendez	C01H	2005 Jul 17
Combined Spectrum	…	3750–6895	51,700	356	523	…	…	This Study	…
…	AAT-echelle	3700–4700	42,000	102[c]	…	…	…	NRB01	…
…	Subaru-HRS	4030–6780	55,000	…	249[d]	3600	…	Ishigaki et al. (2010)	…
…	*Magellan*-MIKE	3350–9100	30,000	51	90	…	…	Frebel et al. (2013)	…

Notes.
[a] S/N per pixel.
[b] This column Proposal ID of archival spectra used in this work or else reference to literature data compared to in the text.
[c] Square root of number of photons per pixel at 4300 Å as described in NRB01.
[d] S/N per resolution element measured at 5800 Å.

analysis. From the ESO science archives, we downloaded UVES spectra of CD −24°17504 in the BLU437 and RED580 setups (see wavelength ranges, resolving power, and S/N information in Table 1). The spectra were obtained in Advanced Data Product format as part of ESO's phase 3 infrastructure.[2] As such, they were reduced with version 5.1.5 of the UVES pipeline and packaged as binary fits files. Fully pipeline-reduced data of CD −24°17504 obtained with HIRES on the Keck telescope were similarly obtained from the KOA, also in the form of binary fits files.

Although archival data given in Table 1 vary by a factor of two in spectral resolution, we chose to maximize S/N at the expense of spectral resolution for this analysis in order to obtain more meaningful upper limits for elements lacking absorption features such as Ba and Eu. These archival data were combined in the following way. Working with each individual exposure, dispersion and flux information for each echelle order were extracted and continuum-normalized using the analysis package "Spectroscopy Made Hard" (SMH; Casey 2014). A low-order cubic spline was used for normalization. Individual orders were then stitched together to create a single continuous one-dimensional (1D) spectrum. Each 1D spectrum was then radial-velocity corrected by cross-correlation against a normalized, rest-frame spectrum of HD 140283 and shifted to rest-frame by scaling the wavelengths without interpolation or rebinning.

A linear wavelength scale was generated with a pixel size set equal to the smallest pixel size of the data, ranging from the shortest to the longest wavelengths shown in Table 1. A sparse matrix of size ($N_{\rm pixels,rebinned}$, $N_{\rm pixels,exposure}$) was then created for each spectrum with a varying Gaussian kernel along the diagonal to convolve the spectral resolution of each exposure to that of the final, rebinned spectrum ($R = 51{,}700$). The kernel values in each column of the matrix were normalized to sum to 1, such that multiplication of each 1D spectrum by this matrix produced a rebinned, convolved, rest-frame spectrum while ensuring no flux information was lost. The rebinned spectra were then combined with each spectrum weighted by its variance.

The Keck HIRES ccd3 spectra, which span $\lambda \sim 7000$–8350 Å, were continuum-normalized, radial-velocity corrected and combined separately within SMH and inspected for the presence of the oxygen triplet at λ7770 Å. No oxygen absorption features were visible, so this spectrum was not analyzed further. Instead, we make use of O measures in the literature in our analysis.

As NRB01 is the work we will most closely compare our results to, it is worthwhile evaluating this new composite spectrum of CD −24°17504 in terms of their figure of merit, defined as $F = (R[\mathrm{S/N}])/\lambda$, where R is spectral resolution, S/N is signal-to-noise ratio, and λ is wavelength. Their echelle spectrum had $F = 830$, nearly a factor of two higher than previous works (NRB01; their Table 1). Here, adopting the nominal $R = 51{,}700$, $F \approx 4400$ at 4300 Å. This value is a factor of five higher than NRB01's value. Details of the NRB01 spectrum are also given in Table 1 for comparison.

3. ANALYSIS

This section describes the details of our analysis of the composite spectrum.

[2] http://www.eso.org/sci/observing/phase3.html

3.1. Equivalenth Width Measurements

For this work, we used the line list compiled in Roederer et al. (2010). EWs of all lines in the line list detected in the spectrum were measured by fitting Gaussians to them in an automatic fashion within SMH. These measures were then checked by eye and remeasured by hand where necessary. For the most part, line measurement uncertainties due to errors in continuum normalization or line blending were minimal. Lines for which element abundances deviated from those of other lines of the same species by more than 2σ were discarded in the abundance analysis (Section 3.2). The line measures used in the abundance analysis are given in Table 2. Lines with EWs as small as 1.5 mÅ were distinguishable from the continuum. Some absorption features in Table 2 were evaluated using spectrum synthesis (see next section) and are likewise indicated.

Lines with very small EW's (<5 mA) are more susceptible to errors in continuum placement than larger lines. Such errors can impact the determination of stellar parameters and element abundances. To better understand this, we measured minimum and maximum EWs for each line corresponding to the minimum and maximum values of the continuum. Half the difference between these is taken as the measurement uncertainty (ΔEW), which is also given in Table 2 for each line. ΔEW ranges from 0.3 to 2.0 mÅ, with a mean of 0.6 mÅ ($\sigma = 0.2$ mÅ). Figure 1 plots the quantity ΔEW/EW versus EW and line excitation potential (EP). As can be seen, most lines have an uncertainty of less then 20%, but the smallest lines can have uncertainties as large as 63%. The bottom panel of Figure 1 shows the potential impact of measurement uncertainties on determination of stellar effective temperature, as the Fe I lines (solid circles) show a slight trend of increasing EW uncertainty with increasing EP. We explore this in more detail in Section 3.2.

Figure 2 shows our EW measures compared to those of three studies from the literature for lines in common: NRB01, Ishigaki et al. (2010, 2012, 2013)[3], and Frebel et al. (2013). Stated again, the figures of merit for the spectra in this work and in NRB01 are 4400 and 830, respectively. The Subaru HDS spectrum used in Ishigaki et al. (2010, 2012, 2013) has $F \approx 2360$, while the *Magellan*-MIKE spectrum of Frebel et al. (2013) has $F \approx 490$. Characteristics of these spectra are also given in Table 1 for comparison.

We have a total of 75 lines in common with the line list of NRB01 (left panels of Figure 2). Our EW measures are generally smaller than theirs (by ~2 mÅ), but agreement is good for the weaker lines. For 17 lines, the difference between our measures and those of NRB01 is 5 mÅ or more. The bottom left panel of Figure 2 shows that 12 of these (predominantly Fe I) lines are located in the region of 3750–3950 Å. This portion of the spectrum is dominated by very strong Balmer absorption lines, which in a star of this temperature have very extended wings. Visual inspection of the lines with the largest measurement differences confirm that the majority of them are located in the wings of these strong absorption lines, indicating that the measurement differences could be due to differences in the continuum normalization.

[3] Although the results of Ishigaki et al. (2012, 2013) appear separate from Ishigaki et al. (2010), they all use the same Subaru HDS spectrum of CD −24°17504. Therefore, we consider the EW measures from all three studies together.

Table 2
Equivalent Widths of CD −24°17504

Species	λ (Å)	EP	log *gf*	EW (mÅ)	ΔEW (mÅ)	log$\epsilon(X)$[a]	ULflag[b]
Li I	6707.800	0.00	0.170	18.5	2.0	1.99	0
CH	4313	…	…	syn	…	6.15	0
CH	4323	…	…	syn	…	6.08	0
Na I	5889.950	0.00	0.108	26.6	1.7	2.61	0
Na I	5895.924	0.00	−0.194	14.6	1.5	2.59	0
Mg I	4057.505	4.35	−0.890	2.1	0.5	4.43	0
Mg I	4167.271	4.35	−0.710	4.2	0.8	4.55	0
Mg I	4702.990	4.33	−0.380	8.8	1.0	4.53	0
Mg I	5172.684	2.71	−0.450	75.2	1.2	4.55	0
Mg I	5183.604	2.72	−0.239	89.4	1.6	4.60	0
Mg I	5528.405	4.34	−0.498	7.4	0.4	4.56	0
Al I	3944.010	0.00	−0.620	syn	…	2.47	0
Al I	3961.520	0.01	−0.340	24.6	1.1	2.35	0
Al I	3961.520	0.01	−0.340	syn	…	2.40	0
Si I	3905.523	1.91	−1.092	52.6	1.3	4.19	0
Si I	3905.523	1.91	−1.092	syn	…	4.20	0
Ca I	4226.730	0.00	0.244	74.9	1.5	3.14	0
Ca I	4283.010	1.89	−0.224	3.7	0.8	3.24	0
Ca I	4318.650	1.89	−0.210	3.2	0.4	3.17	0
Ca I	4425.440	1.88	−0.358	3.0	0.6	3.27	0
Ca I	4434.960	1.89	−0.010	4.9	0.5	3.15	0
Ca I	4435.690	1.89	−0.519	2.2	0.7	3.30	0
Ca I	4454.780	1.90	0.260	8.7	0.6	3.16	0
Ca I	5588.760	2.52	0.210	3.3	1.5	3.29	0
Ca I	6122.220	1.89	−0.315	2.6	0.6	3.12	0
Ca I	6162.170	1.90	−0.089	4.0	0.5	3.09	0
Ca I	6439.070	2.52	0.470	3.3	0.6	3.00	0
Sc II	4246.820	0.32	0.240	syn	…	−0.01	0
Sc II	4314.083	0.62	−0.100	syn	…	−0.06	0
Sc II	4324.998	0.59	−0.440	syn	…	−0.22	0
Sc II	4400.389	0.61	−0.540	syn	…	−0.01	0
Sc II	4415.540	0.59	−0.670	syn	…	0.07	0
Ti I	3989.760	0.02	−0.062	3.8	0.8	2.13	0
Ti I	3998.640	0.05	0.010	5.2	0.7	2.23	0
Ti I	4533.249	0.85	0.532	3.6	0.3	2.25	0
Ti I	4534.780	0.84	0.336	2.1	0.2	2.19	0
Ti II	3913.461	1.12	−0.420	22.7	1.0	1.94	0
Ti II	4012.396	0.57	−1.750	4.2	0.6	1.89	0
Ti II	4163.634	2.59	−0.400	1.8	0.3	2.03	0
Ti II	4290.219	1.16	−0.930	7.6	0.4	1.88	0
Ti II	4300.049	1.18	−0.490	16.4	1.0	1.85	0
Ti II	4395.031	1.08	−0.540	19.4	1.1	1.89	0
Ti II	4399.765	1.24	−1.190	3.5	0.3	1.85	0
Ti II	4417.714	1.17	−1.190	3.6	0.4	1.79	0
Ti II	4443.801	1.08	−0.720	14.9	0.6	1.92	0
Ti II	4450.482	1.08	−1.520	2.9	0.6	1.95	0
Ti II	4468.517	1.13	−0.600	15.0	0.8	1.85	0
Ti II	4501.270	1.12	−0.770	12.7	0.7	1.92	0
Ti II	4533.960	1.24	−0.530	13.4	0.5	1.82	0
Ti II	4563.770	1.22	−0.960	9.1	0.5	2.03	0
Ti II	4571.971	1.57	−0.320	12.7	0.5	1.88	0
Ti II	5188.687	1.58	−1.050	2.2	0.4	1.79	0
Cr I	4254.332	0.00	−0.114	19.3	0.5	2.13	0
Cr I	4274.800	0.00	−0.220	16.6	0.7	2.16	0
Cr I	4289.720	0.00	−0.370	13.8	0.6	2.20	0
Cr I	5206.040	0.94	0.020	7.0	0.7	2.30	0
Cr I	5208.419	0.94	0.160	10.2	0.6	2.35	0
Mn I	4030.753	0.00	−0.480	syn	…	2.00	0
Mn I	4033.062	0.00	−0.618	syn	…	2.04	0
Mn I	4034.483	0.00	−0.811	syn	…	2.05	0
Fe I	3786.677	1.01	−2.185	3.1	0.6	4.03	0
Fe I	3787.880	1.01	−0.838	38.1	0.6	4.05	0
Fe I	3805.343	3.30	0.313	7.0	0.5	4.00	0
Fe I	3815.840	1.48	0.237	64.5	1.1	4.04	0

Table 2
(Continued)

Species	λ (Å)	EP	log gf	EW (mÅ)	ΔEW (mÅ)	log$\epsilon(X)$[a]	ULflag[b]
Fe I	3820.425	0.86	0.157	82.0	0.8	4.12	0
Fe I	3824.444	0.00	−1.360	61.3	0.6	4.23	0
Fe I	3825.881	0.91	−0.024	70.1	0.7	4.00	0
Fe I	3827.823	1.56	0.094	50.1	0.8	3.91	0
Fe I	3839.256	3.05	−0.330	2.6	0.4	3.96	0
Fe I	3840.438	0.99	−0.497	44.6	0.6	3.84	0
Fe I	3841.048	1.61	−0.044	41.1	0.7	3.87	0
Fe I	3846.800	3.25	−0.020	3.8	0.8	4.00	0
Fe I	3849.967	1.01	−0.863	38.1	0.7	4.06	0
Fe I	3850.818	0.99	−1.745	10.2	0.8	4.12	0
Fe I	3852.573	2.18	−1.180	2.7	0.5	4.01	0
Fe I	3856.372	0.05	−1.280	64.3	0.8	4.28	0
Fe I	3859.911	0.00	−0.710	86.3	0.6	4.32	0
Fe I	3865.523	1.01	−0.950	33.9	0.7	4.06	0
Fe I	3867.216	3.02	−0.450	3.1	0.5	4.13	0
Fe I	3878.018	0.96	−0.896	37.6	0.5	4.04	0
Fe I	3878.573	0.09	−1.380	57.1	0.7	4.20	0
Fe I	3895.656	0.11	−1.668	38.2	0.7	4.03	0
Fe I	3899.707	0.09	−1.515	48.9	1.0	4.11	0
Fe I	3902.946	1.56	−0.442	33.1	0.7	4.03	0
Fe I	3917.181	0.99	−2.155	4.3	0.5	4.11	0
Fe I	3920.258	0.12	−1.734	41.0	0.8	4.16	0
Fe I	3922.912	0.05	−1.626	48.9	0.9	4.18	0
Fe I	3977.741	2.20	−1.120	3.5	0.6	4.10	0
Fe I	4005.242	1.56	−0.583	29.8	0.8	4.08	0
Fe I	4021.866	2.76	−0.730	2.7	0.6	4.10	0
Fe I	4045.812	1.49	0.284	69.4	0.8	4.15	0
Fe I	4062.441	2.85	−0.860	2.0	0.5	4.17	0
Fe I	4063.594	1.56	0.062	57.2	0.7	4.10	0
Fe I	4067.978	3.21	−0.470	1.6	0.4	4.01	0
Fe I	4071.738	1.61	−0.008	52.3	0.7	4.08	0
Fe I	4076.629	3.21	−0.370	1.6	0.3	3.91	0
Fe I	4132.058	1.61	−0.675	25.3	0.9	4.11	0
Fe I	4134.678	2.83	−0.649	3.6	0.5	4.20	0
Fe I	4136.998	3.42	−0.450	1.4	0.5	4.12	0
Fe I	4143.414	3.05	−0.200	5.3	0.5	4.13	0
Fe I	4143.868	1.56	−0.511	33.6	0.7	4.09	0
Fe I	4147.669	1.48	−2.071	1.8	0.4	4.09	0
Fe I	4153.899	3.40	−0.320	1.8	0.5	4.08	0
Fe I	4154.498	2.83	−0.688	2.0	0.5	3.98	0
Fe I	4154.805	3.37	−0.400	1.5	0.6	4.05	0
Fe I	4156.799	2.83	−0.808	2.3	0.7	4.16	0
Fe I	4157.780	3.42	−0.403	2.6	0.5	4.34	0
Fe I	4174.913	0.91	−2.938	1.3	0.5	4.26	0
Fe I	4181.755	2.83	−0.371	6.4	0.7	4.19	0
Fe I	4184.892	2.83	−0.869	2.0	0.4	4.16	0
Fe I	4187.039	2.45	−0.514	7.9	0.5	4.08	0
Fe I	4187.795	2.42	−0.510	7.8	0.6	4.04	0
Fe I	4191.430	2.47	−0.666	6.1	0.3	4.13	0
Fe I	4195.329	3.33	−0.492	1.8	0.5	4.18	0
Fe I	4199.095	3.05	0.156	9.5	0.8	4.05	0
Fe I	4202.029	1.49	−0.689	29.6	0.9	4.10	0
Fe I	4216.184	0.00	−3.357	2.8	0.4	4.17	0
Fe I	4222.213	2.45	−0.914	3.2	0.6	4.06	0
Fe I	4227.427	3.33	0.266	8.2	0.7	4.12	0
Fe I	4233.603	2.48	−0.579	6.5	0.7	4.08	0
Fe I	4238.810	3.40	−0.233	2.1	0.7	4.05	0
Fe I	4247.426	3.37	−0.240	2.7	0.9	4.15	0
Fe I	4250.119	2.47	−0.380	9.3	0.7	4.04	0
Fe I	4250.787	1.56	−0.713	24.9	0.5	4.08	0
Fe I	4260.474	2.40	0.077	24.2	0.7	4.03	0
Fe I	4271.154	2.45	−0.337	11.6	0.8	4.09	0
Fe I	4271.760	1.49	−0.173	53.8	0.6	4.15	0
Fe I	4282.403	2.18	−0.779	7.3	0.5	4.06	0

Table 2
(Continued)

Species	λ (Å)	EP	log *gf*	EW (mÅ)	ΔEW (mÅ)	log$\epsilon(X)$[a]	ULflag[b]
Fe I	4325.762	1.61	0.006	53.7	0.3	4.07	0
Fe I	4352.735	2.22	−1.290	2.2	0.9	4.05	0
Fe I	4375.930	0.00	−3.005	5.9	0.5	4.13	0
Fe I	4383.545	1.48	0.200	69.4	0.7	4.17	0
Fe I	4404.750	1.56	−0.147	52.4	0.7	4.14	0
Fe I	4415.122	1.61	−0.621	29.9	0.5	4.13	0
Fe I	4427.310	0.05	−2.924	6.7	0.6	4.16	0
Fe I	4442.339	2.20	−1.228	3.1	0.6	4.16	0
Fe I	4447.717	2.22	−1.339	2.5	0.4	4.15	0
Fe I	4459.118	2.18	−1.279	3.3	0.6	4.18	0
Fe I	4461.653	0.09	−3.194	4.0	0.7	4.22	0
Fe I	4466.552	2.83	−0.600	2.5	1.0	3.95	0
Fe I	4476.019	2.85	−0.820	2.9	0.6	4.27	0
Fe I	4528.614	2.18	−0.822	7.6	0.6	4.10	0
Fe I	4531.148	1.48	−2.101	1.7	0.5	4.05	0
Fe I	4602.941	1.49	−2.208	1.2	0.6	4.00	0
Fe I	4871.318	2.87	−0.362	4.3	0.6	3.99	0
Fe I	4890.755	2.88	−0.394	4.3	0.5	4.03	0
Fe I	4891.492	2.85	−0.111	9.1	0.4	4.07	0
Fe I	4903.310	2.88	−0.926	1.3	0.5	4.03	0
Fe I	4918.994	2.85	−0.342	5.1	0.6	4.03	0
Fe I	4920.503	2.83	0.068	13.1	0.7	4.06	0
Fe I	5012.068	0.86	−2.642	1.9	0.9	4.03	0
Fe I	5083.339	0.96	−2.842	1.7	0.7	4.27	0
Fe I	5171.596	1.49	−1.721	4.3	0.7	4.05	0
Fe I	5192.344	3.00	−0.421	3.2	0.5	4.02	0
Fe I	5194.942	1.56	−2.021	1.9	1.2	4.05	0
Fe I	5232.940	2.94	−0.057	8.8	0.6	4.07	0
Fe I	5266.555	3.00	−0.385	3.5	0.7	4.03	0
Fe I	5269.537	0.86	−1.333	34.4	1.0	4.20	0
Fe I	5328.039	0.92	−1.466	13.5	0.6	3.81	0
Fe I	5371.489	0.96	−1.644	8.9	0.7	3.81	0
Fe I	5383.369	4.31	0.645	2.7	0.7	4.07	0
Fe I	5397.128	0.92	−1.982	9.8	1.0	4.16	0
Fe I	5405.775	0.99	−1.852	11.0	0.6	4.15	0
Fe I	5415.199	4.39	0.643	2.5	0.5	4.11	0
Fe I	5424.068	4.32	0.520	3.5	1.1	4.32	0
Fe I	5429.696	0.96	−1.881	11.1	1.0	4.16	0
Fe I	5434.524	1.01	−2.126	5.6	1.1	4.12	0
Fe I	5446.917	0.99	−1.910	10.7	1.3	4.20	0
Fe I	5455.609	1.01	−2.090	7.0	0.7	4.19	0
Fe I	5497.516	1.01	−2.825	1.0	0.5	4.05	0
Fe I	5506.779	0.99	−2.789	1.6	0.3	4.20	0
Fe I	5586.756	3.37	−0.144	3.2	0.8	4.07	0
Fe I	5615.644	3.33	0.050	4.7	0.8	4.02	0
Fe II	4233.170	2.58	−1.970	6.4	1.3	4.08	0
Fe II	4522.630	2.84	−2.250	2.9	0.7	4.21	0
Fe II	4583.840	2.81	−1.930	5.0	0.7	4.11	0
Fe II	4923.930	2.89	−1.320	12.4	0.8	4.00	0
Fe II	5018.450	2.89	−1.220	16.4	1.1	4.04	0
Co I	3845.468	0.92	0.010	7.6	1.0	2.01	0
Co I	3873.120	0.43	−0.660	9.0	0.9	2.31	0
Co I	3995.306	0.92	−0.220	7.2	0.8	2.20	0
Co I	4121.318	0.92	−0.320	4.8	0.6	2.10	0
Ni I	3783.520	0.42	−1.420	16.2	1.1	3.20	0
Ni I	3807.140	0.42	−1.220	19.6	0.7	3.09	0
Ni I	3858.301	0.42	−0.951	32.6	0.8	3.15	0
Ni I	5476.900	1.83	−0.890	4.3	0.4	3.19	0
Zn I	4810.528	4.08	−0.137	3.1	1.0	2.15	0
Sr II	4077.714	0.00	0.150	5.5	0.6	−1.81	0
Sr II	4077.714	0.00	0.150	syn	…	−1.82	0
Sr II	4215.524	0.00	−0.180	3.1	0.7	−1.75	0
Sr II	4215.524	0.00	−0.180	syn	…	−1.80	0
Y II	3788.694	0.10	−0.140	<1.0	…	< −1.36	1

Table 2
(Continued)

Species	λ (Å)	EP	log *gf*	EW (mÅ)	ΔEW (mÅ)	log$\epsilon(X)$[a]	ULflag[b]
Zr II	4208.977	0.71	−0.460	<1.0	…	<0.08	1
Ba II	4554.033	0.00	0.163	<1.0	…	<−2.28	1
La II	4123.220	0.32	0.130	<1.0	…	<−1.08	1
Eu II	4129.700	0.00	0.220	<1.0	…	<−1.73	1

Notes.
[a] LTE abundance.
[b] Upper limit flag: 1 = yes, 0 = no.

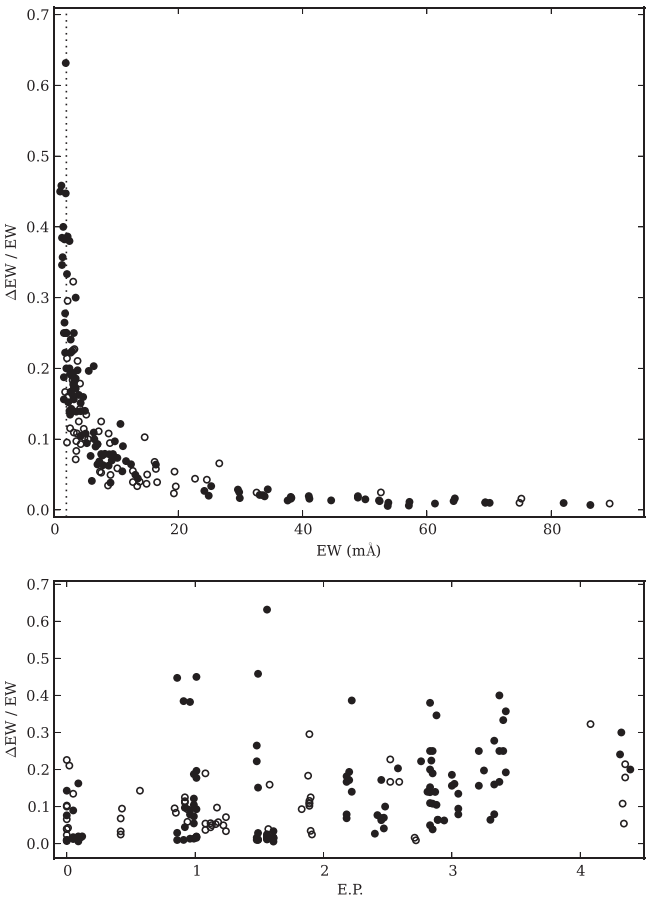

Figure 1. Fraction EW uncertainty (ΔEW/EW) as a function of line strength (top panel) and line EP (bottom panel). Fe I and Fe II lines are indicated by black circles, and non-Fe species are given as open circles. To guide the eye, the dotted line in the top panel indicates a line strength of 2 mÅ.

The remaining five lines with large measurement differences were not located near any strong absorption features. In each case, we could not reduce the EW measurement difference by adjustment of the continuum; to make the lines as strong as measured by NRB01 required measuring the line well above the location of the continuum. We therefore attribute the measurement differences to S/N differences.

The right panels of Figure 2 compare our EW measures with those measured in a MIKE spectrum of CD −24°17504 from our earlier work (Frebel et al. 2013). Here, the agreement is less good, with a larger mean offset (5.4 mÅ) and substantially larger scatter. We inspected each line for which the EW difference was larger than 3 mÅ (45 lines) in the MIKE spectrum from Frebel et al. (2013), which has both lower S/N and lower resolution than in this work (Table 1). Only nine of these lie near strong Balmer features. For 14 lines, we found that the EW values were consistent with each other considering the S/N of the region; that is, that slight adjustments of the continuum level within its uncertainty got the EW measures to agree. For 15 further lines, similar adjustments decreased the EW discrepency by 50% or more. For some remaining lines, EW discrepencies could not be decreased.

Finally, the middle panels compare our measures to those in Ishigaki et al. (2010, 2012, 2013). Though we only have 39 lines in common, this study is in a sense most similar to ours in that their analysis was based on data superior in resolution ($R \sim 55{,}000$) and of high S/N (~250; Table 1). As can be seen, agreement is excellent, with a mean offset of −0.2 mÅ. In summary, the differences in EW measures among these different studies is representative of the varying quality of the data they came from.

3.2. Determination of Stellar Parameters

For this work, we make use of the Castelli–Kurucz grid of 1D plane-parallel model atmospheres (Castelli & Kurucz 2004) with no-overshoot and the local thermodynamic equilibrium (LTE) analysis code MOOG (2011 May version, Sneden 1973) that includes treatment of Rayleigh scattering (Sobeck et al. 2011). Stellar parameters for CD −24°17504 were determined via classical spectroscopic techniques which use the EWs of Fe I and Fe II lines described in the previous section. Effective temperature was determined by reducing any trend of Fe I line abundance with EP, and microturbulent velocity was adjusted to remove Fe I line abundance trends with reduced EW. Surface gravity, log *g*, was adjusted until the average Fe I and Fe II agreed within 0.05 dex. The metallicity of the model atmosphere ([M/H]) was also adjusted as needed. This process was iterated upon until all three requirements were satisfied, and then we applied the empirical correction to $T_{\rm eff}$ described in Frebel et al. (2013). The resulting stellar parameters are $T_{\rm eff} = 6228$ K, $\log g = 3.90$, $v_{\rm t} = 1.25$ km s^{-1}, and [Fe/H] = −3.41 ($\sigma = 0.10$) dex (Table 3).

Based on an analysis of a MIKE spectrum of CD −24°17504 described earlier, we found $T_{\rm eff}$ and $v_{\rm t}$ values in good agreement with those found here: 6259 K and 1.40 km s^{-1}, respectively (Frebel et al. 2013). However, the surface gravity in that work was 0.25 dex lower ($\log g = 3.65$), and [Fe/H] was 0.18 dex higher (−3.23). In Frebel et al. (2013), the Fe II abundance was based on measures of two lines in CD −24°17504, the EWs of both being ~50% larger than found in this study (see previous

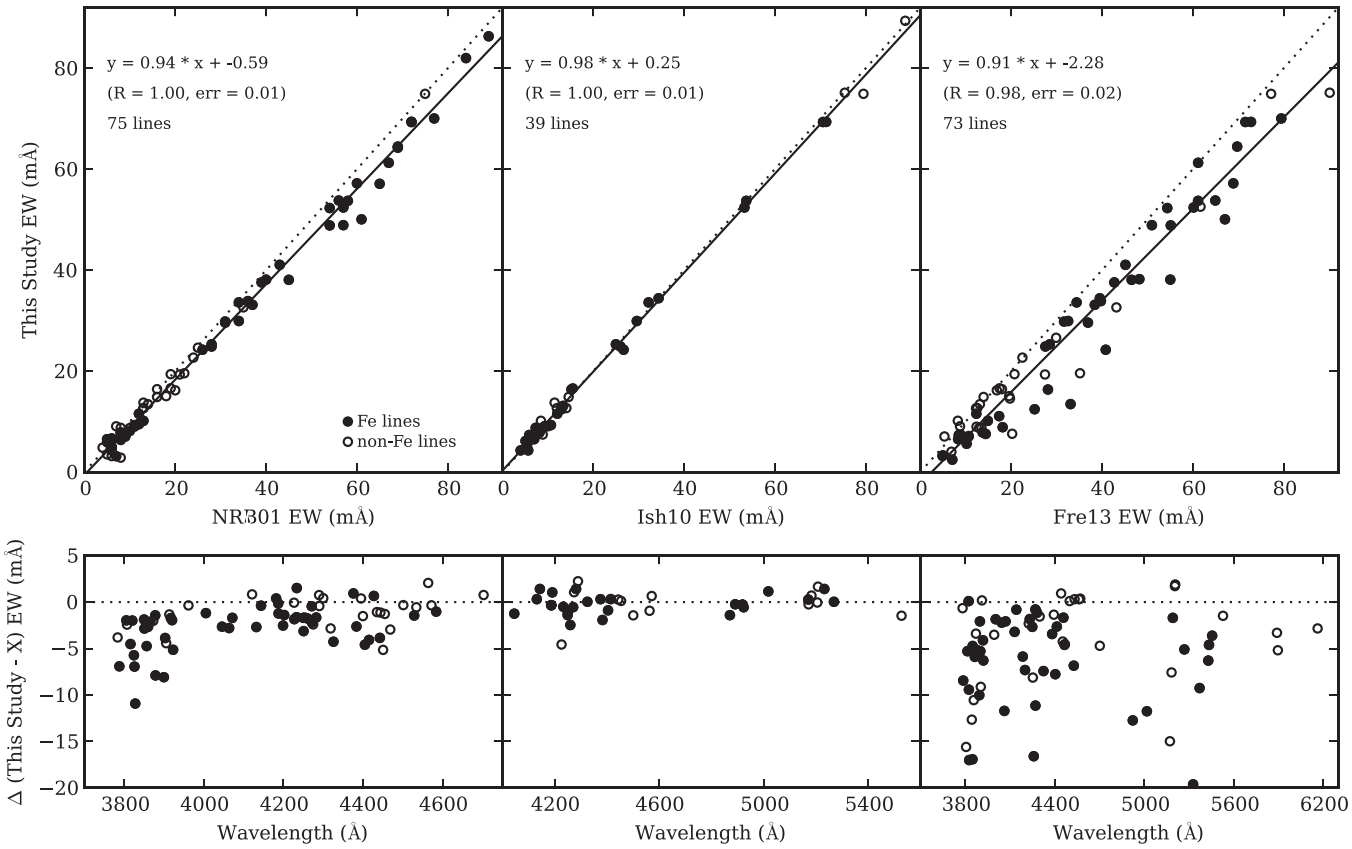

Figure 2. Comparison of EWs measured in this study to those in the literature. In the top panels, dotted lines indicate a 1:1 correlation, while solid lines are lines of best fit through the data. Fe I and Fe II lines are indicated by filled circles. The bottom panels show the difference between EW measures as a function of wavelength.

section). To investigate the matter, we adjusted the measures of these two lines in their MIKE spectrum within comfortable limits of the noise level and repeated the stellar parameter determination, resulting in parameters $T_{\rm eff}$ = 6259 K, $\log g$ = 4.35, $v_{\rm t}$ = 1.2 km s^{-1}, and [Fe/H] = −3.22. This 0.7 dex adjustment to surface gravity illustrates the necessity of having several well-measured Fe II lines for spectroscopic stellar parameter determination. The ∼0.2 dex higher metallicity compared to that found in this study can likewise be attributed to systematically larger EWs.

Numerous stellar parameter determinations for CD −24°17504 based on different techniques can be found in the literature. Figure 3 shows the position of CD −24°17504 in the Hertzsprung–Russell diagram using stellar parameters from various studies, which are also listed in Table 3. Filled symbols represent studies that determined stellar parameters spectroscopically, similar to that described above. Open symbols indicate studies that determined $T_{\rm eff}$ via photometry and color-temperature calibrations, or via fitting the wings of Balmer lines. In these cases, $\log g$ was either determined via matching to theoretical isochrones or by ionization balance of Fe I and Fe II lines. Figure 3 and Table 3 clearly show the range of stellar parameters these same few methods, used by different authors, provide. Indeed, CD −24°17504 can be classified as either a main sequence dwarf star or a subgiant.

It is also well established that the assumption of LTE can introduce systematic offsets into a classical spectroscopic analysis, and that these systematics increase with decreasing stellar metallicity and decreasing $\log g$ (e.g., Thévenin & Idiart 1999; Asplund 2005; Lind et al. 2012). To mitigate these effects, we determined stellar parameters for CD −24°17504 following a method described in Ruchti et al. (2013) and starting with our empirically calibrated spectroscopic $T_{\rm eff}$ (6228 K).[4] We then determined Δ[Fe/H] (NLTE −LTE) for Fe I lines in our line list that were present in the INSPECT database,[5] adopting $T_{\rm eff}$ = 6228 K, $\log g$ = 4.0, [Fe/H] = −3.4, and $v_{\rm t}$ = 1.25 km s^{-1}(Bergemann et al. 2012b; Lind et al. 2012). For the 18 Fe I lines, the average Δ[Fe/H] = +0.12 dex (σ = 0.04). Therefore, $[{\rm Fe\,I/H}]_{\rm LTE} = -3.41$ corresponds to $[{\rm Fe\,I/H}]_{\rm NLTE} = -3.29$. Next, $\log g$ was adjusted to achieve [Fe II/H] = −3.29, and $v_{\rm t}$ was adjusted to remove any trends of Fe I abundance with line strength. The resulting "NLTE" stellar parameters are $T_{\rm eff}$ = 6228 K, $\log g$ = 4.23, $v_{\rm t}$ = 1.00 km s^{-1}, and [Fe/H] = −3.29 (Table 3).

The LTE and "NLTE" parameters determined here for CD −24°17504 are indicated by a black diamond and black star in Figure 3, respectively. As can be seen, CD −24° 17504 appears to be a dwarf star or a subgiant star depending on the assumption of LTE for Fe I lines in the determination of $\log g$ via ionization balance. Our "NLTE" parameters are more consistent with those found photometrically, the majority of which indicate CD −24°17504 is a dwarf star with $\log g > 4$. For the rest of this paper, we will mostly focus on the LTE parameters and subsequent element abundances for comparison

[4] Recall that this calibration places spectroscopically determined $T_{\rm eff}$ values on a rough "photometric" scale, and that this correction increases with decreasing $T_{\rm eff}$ (and decreasing $\log g$)—similar to the direction that NLTE–LTE differences increase. Therefore this empirical calibration "softens the blow" of using purely spectroscopic techniques.

[5] http://www.inspect-stars.com

Table 3
Atmospheric Parameters for CD −24°17504 in this Study and in the Literature

$T_{\rm eff}$ (K)	log g (dex)	$v_{\rm t}$ (km s^{-1})	[Fe/H] (dex)	Method	References
6228	3.90	1.25	−3.41	spec[a], LTE	This Study
6228	4.23	1.00	−3.29	spec[a], NLTE	This Study
6259	3.65	1.40	−3.23	spec[a]	Frebel et al. (2013)
6236	3.70	1.60	−3.23	phot	Yong et al. (2013a)
5821	3.50	1.22	−3.66	spec	Ishigaki et al. (2010)
6456	4.74	1.50	−3.20	comb	Ishigaki et al. (2012)
6451	4.13	…	−3.34	phot	Meléndez et al. (2010)
6180	4.40	1.50	−3.40	balm	Aoki et al. (2009)
6070	3.57	1.30	−3.35	comb	Hosford et al. (2009)
5942	4.05	1.50	−3.42	spec	Rich & Boesgaard (2009)
6338	4.32	1.50	−3.21	balm	Nissen et al. (2007)
6070	4.20	1.80	−3.45	phot	Arnone et al. (2005)
6212	4.13	1.00	−2.99	phot	Bihain et al. (2004)
6212	4.13	…	−3.32	phot	Israelian et al. (2001)
6070	3.60	1.40	−3.37	comb	Norris et al. (2001)
6300	4.50	1.00	−3.30	phot	Primas et al. (2000)
6100	4.00	1.50	−3.70	balm	Spite et al. (1996)

Notes. Methods for determining stellar parameters range from classical spectroscopic methods ("spec"), use of color-temperature relations ("phot"), or fitting of Balmer line absorption wings ("balm"). In the latter two methods, log g is often determined by comparison to theoretical isochrones, but in some cases, is determined by ionization balance. These cases are noted as "comb," for combination of methods.
[a] Parameters determined spectroscopically, but with correction applied to $T_{\rm eff}$. See text for more information.

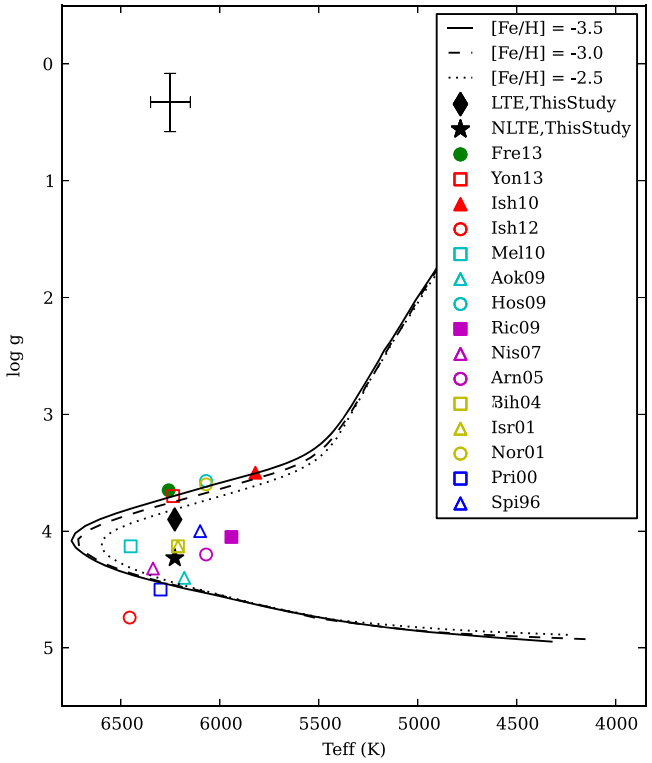

Figure 3. Location of CD −24°17504 in the Hertzsprung–Russell diagram using stellar parameters from different studies. For reference, 12 Gyr Yale-Yonseii isochrones with [α/Fe] = +0.40 and [Fe/H] = −2.5, −3.0, and −3.5 are shown as dotted, dashed, and solid lines, respectively (Kim et al. 2002). Filled symbols indicate that stellar parameters were determined spectroscopically; open symbols indicate other methods were used. The parameters found in this work are indicated by a filled diamond (LTE) and star ("NLTE"), respectively. See text for details. Note that the literature results assume LTE; references are given in Table 3.

to literature values (which by and large assume LTE), but we will include abundances determined with the "NLTE" parameters for reference. Additional NLTE corrections to individual elements will also be discussed were necessary and available. Finally, we note this analysis did not consider possible 1D–3D effects and the possible systematic biases introduced by our assumption of plane-parallel model atmospheres. 3D effects can be large for stars of this metallicity, but exploration of them except for specific elements is beyond the scope of this paper.

3.3. Element Abundance Analysis

Abundances for the following elements were determined using measured EWs and the LTE and "NLTE" sets of stellar parameters described above: Na I, Mg I, Si I, Ca I, Ti I, Ti II, Cr I, Co I, Ni I, and Zn I. Each line measurement was visually inspected and strong outliers were removed. Spectrum synthesis was used to determine abundances for Li, C, Sc II, Mn I, and Sr II. Sets of three synthetic spectra of varying element abundance were generated using MOOG and plotted over the observed spectrum. The synthetic spectra were convolved with a Gaussian to match the resolution of the data and the continuum level was adjusted where necessary. The element abundance was then varied until the best match was found. This was done by visually evaluating the residuals of the (synthetic-observed) data.

Upper limits to element abundances were calculated based on the noise level of the spectrum. The σ of the noise level can be assessed using the Cayrel formula: $\sigma \approx 1.5 \times (\mathrm{S/N})^{-1} \times \sqrt{(\mathrm{FWHM} \times \delta \mathrm{x})}$, where S/N is the signal-to-noise ratio, FWHM is the typical full width at half maximum of absorption lines in that part of the spectrum, and δx is the spectral dispersion (Cayrel et al. 1988). Typical values were ∼0.15 mÅ. The corresponding 3σ upper limit EW of 0.5 mÅ is comparable to the mean ΔEW uncertainty of 0.6 mÅ discussed earlier. However, we have opted to set the upper limit EW to 1 mÅ, the minimum accepted value for detected lines (Table 2). This value was used to determine upper limits to the abundances of Y II (3788 Å), Zr II (4209 Å), Ba II (4554 Å), La II (4123 Å), and Eu II (4129 Å). The element abundances corresponding to these upper limit EWs were found using either the "blends" or "abfind" routine in MOOG, for lines with and without hyperfine or isotopic splitting, respectively. In the case of Ba, we adopted the r-process only isotopic ratio. Individual line LTE abundances are given in Table 2.

Figure 4 shows the results of this upper limit analysis, as well as spectrum synthesis of the region around the Sr II 4077 Å feature. For the Sr synthesis, synthetic spectra with logϵ(Sr) ± 0.3 dex around the best-fit abundance are shown by red lines. For all the other species, synthetic spectra with the abundances determined from the 1 mÅ EW upper limits are shown as black solid lines, while the red lines represent synthetic spectra with abundances found using EWs of 0.5 and 1.5 mÅ. As can be seen, 1 mÅ is a reasonable upper limit in each region of the spectrum.

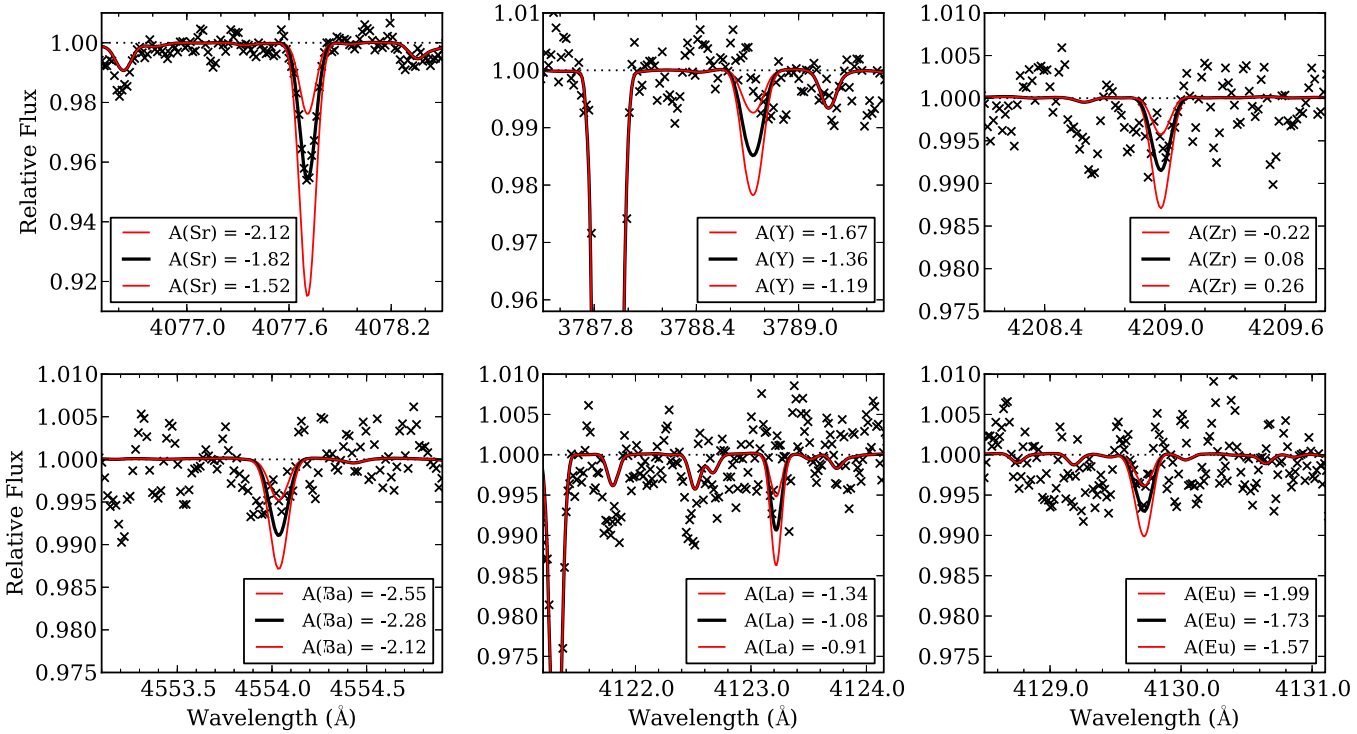

Figure 4. Portions of the spectrum of CD −24°17504 at the locations of various neutron-capture element absorption features. The only element detected, Sr, was analyzed with spectrum synthesis. The best-fit synthetic spectrum is indicated by a black solid line, with spectra illustrating logϵ(Sr) ≡ A(Sr) ± 0.3 dex are shown as red lines. For the other elements, synthetic spectra with element abundances determined adopting an EW upper limit of 1 mÅ are given by black lines, with red lines representing synthetic spectra with abundances determined using EWs of 0.5 and 1.5 mÅ.

It has been noted in the literature that the Mn I resonance lines at 4030 Å indicate systematically lower Mn abundances than do weaker non-resonance lines (Cayrel et al. 2004; Lai et al. 2008). Our investigations of these offsets in HD 122563 and HD 140283 found an offset of +0.30 dex (in the sense non-resonance minus resonance), in agreement with literature studies. Therefore, we have corrected the abundances determined from Mn I 4030 Å, 4033 Å, and 4034 Å by +0.30 dex. The individual Mn line abundances in Tables 2 include this offset. Bergemann & Gehren (2008) have shown that this 0.3 dex offset can be attributed to NLTE effects on the resonance lines.

Abundance results are presented in Table 6 adopting the LTE stellar parameters, while the results of the "NLTE" analysis are shown in Table 7. The adopted solar abundances are those of Asplund et al. (2009).

3.4. Analysis of the Uncertainties

We evaluated the uncertainties in the stellar parameters of CD −24°17504 in the following way. $T_{\rm eff}$ and $v_{\rm t}$ were adjusted until slopes were introduced into relations of Fe I line abundance with EP and reduced EW that exceeded tolerable levels given the 1σ dispersion in Fe I line abundances. Surface gravity was adjusted until [Fe II/H] − [Fe/H] = $(\sigma^2_{\rm Fe\,I} + \sigma^2_{\rm Fe\,II})^{1/2}$. The results are $\Delta T_{\rm eff}$ = 60 K, $\Delta \log g$ = 0.30, and $\Delta v_{\rm t}$ = 0.1 km s^{-1}. These values are consistent with those found using the empirical relations of Roederer et al. (2014): $\Delta T_{\rm eff}$ = 61 K (40 K), $\Delta v_{\rm t}$ = 0.05 km s^{-1}(0.15 km s^{-1}) for the subgiant (main-sequence) star relations. Finally, we set Δ[M/H] = $\sigma_{\rm Fe\,I}$.

We evaluated the sensitivity of these parameters to uncertainties in EW measures in a Monte Carlo fashion. Starting with the EW measures in Table 2, we generated Gaussian distributions of EWs for each line with the FWHM equal to the line's ΔEW. We then randomly selected an EW from these distributions and generated 10 sets of EW measures. For the smallest Fe I lines, if the resulting EW was smaller than 1 mÅ, it was excluded (generally no more than 2–3 lines were excluded). Starting from the original stellar parameters (before application of the $T_{\rm eff}$ correction), $T_{\rm eff}$, $v_{\rm t}$ and log g were varied to establish ionization and excitation balance and to remove abundance trends with line strength. The empirical $T_{\rm eff}$ correction was then applied and final adjustments to log g, $v_{\rm t}$, and [M/H] were performed. The difference between the resulting parameters and the LTE parameters in Table 3 for each of the 10 trials is given in Table 4. Considering the

Table 4
Uncertainties in Stellar Parameters Due to Errors in Fe I, Fe II EWs

Run	$\Delta T_{\rm eff}$ (K)	$\Delta \log g$ (dex)	$\Delta v_{\rm t}$ (km s^{-1})	Δ[Fe/H] (dex)	# Fe I	# Fe II
01	−68	−0.18	+0.00	−0.04	112	5
02	+76	−0.02	+0.06	+0.07	112	5
03	−67	−0.24	+0.06	−0.06	109	5
04	+13	+0.02	+0.05	+0.01	110	5
05	−51	−0.25	+0.00	−0.03	112	5
06	+123	+0.48	+0.04	+0.10	110	5
07	+37	+0.09	+0.08	+0.02	112	5
08	−71	−0.05	−0.09	−0.04	110	5
09	−6	−0.03	+0.08	−0.01	110	5
10	−74	−0.13	−0.02	−0.05	113	5
Ave.	59	0.15	0.05	0.04	…	…
σ	34	0.15	0.03	0.03	…	…

Table 5
Log(ϵ) Abundance Uncertainties due to Atmospheric Parameters

Species	σ(EW)[a]	$\Delta T_{\rm eff}$(K) +84 K	Δlog g +0.34 dex	$\Delta v_{\rm t}$ +0.11 km s^{-1}	Δ[M/H] +0.11 dex	Total
Li I	0.03[b]	+0.06	+0.00	+0.00	+0.00	0.07
CH	0.10[b]	+0.15	−0.15	+0.00	+0.00	0.23
Na I	0.02	+0.06	−0.01	+0.00	+0.00	0.06
Mg I	0.07	+0.04	−0.03	−0.01	+0.00	0.09
Al I	0.09	+0.05	−0.01	−0.01	+0.00	0.10
Si I	0.15[c]	+0.05	−0.01	−0.02	−0.01	0.16
Ca I	0.08	+0.05	−0.01	+0.00	+0.01	0.10
Sc II	0.10	+0.04	+0.11	+0.00	+0.00	0.15
Ti I	0.05	+0.07	+0.00	+0.00	+0.01	0.09
Ti II	0.11	+0.04	+0.12	+0.00	+0.00	0.18
Cr I	0.09	+0.07	−0.01	+0.00	+0.00	0.11
Mn I	0.20	+0.08	+0.00	+0.00	+0.01	0.22
Fe I	0.10	+0.06	−0.01	−0.01	+0.00	0.12
Fe II	0.07	+0.01	+0.12	+0.00	+0.00	0.14
Co I	0.11	+0.07	+0.00	+0.00	+0.00	0.13
Ni I	0.06	+0.08	+0.01	+0.00	+0.01	0.10
Zn I	0.15[c]	+0.04	+0.03	+0.00	+0.00	0.16
Sr II	0.10	+0.05	+0.11	+0.00	+0.00	0.16
Y II	0.18[d]	+0.05	+0.11	+0.00	+0.00	0.22
Zr II	0.18[d]	+0.04	+0.11	+0.00	+0.00	0.21
Ba II	0.16[d]	+0.05	+0.10	+0.10	+0.00	0.20
La II	0.17[d]	+0.03	+0.11	−0.01	−0.01	0.21
Eu II	0.16[d]	+0.05	+0.11	+0.00	+0.00	0.20

Notes.
[a] The maximum of the standard deviation of individual line element abundances or the abundance sensitivity to EW uncertainties.
[b] Sensitivity of abundance to continuum placement.
[c] Value given to measures based on one line.
[d] EW uncertainty set to 0.5 mÅ. See text for more information.

magnitudes of the differences, they are on average 59 (σ = 34) K for $T_{\rm eff}$, 0.15 (σ = 0.15) dex for log g, 0.05 (σ = 0.03) km s^{-1} for $v_{\rm t}$, and 0.04 (σ = 0.03) dex for [Fe/H]. These values along with the uncertainties in the previous paragraph were added in quadrature to determine the total uncertainties in the spectroscopic parameters: 84 K for $T_{\rm eff}$, 0.34 dex for log g, 0.11 km s^{-1} for $v_{\rm t}$, and 0.11 dex for [M/H]. The sensitivity of element abundances to these parameter uncertainties were determined by varying each parameter by its uncertainty independently. Table 5 gives the abundance uncertainties for each element.

For the non-Fe species, we determined the uncertainty in the abundance due to EW error by using the 10 variations of the line list and determined individual line abundances using the LTE stellar parameters. The mean element abundances were then compared to those in Table 6. Typical differences were 0.02 to 0.03 dex, but were as large as 0.14 dex in the case of the single Zn I line measured. We take the maximum of either this difference or the standard deviation of the line abundances in Table 6 as the element abundance sensitivity to EW uncertainty. The total sensitivity of element abundances to stellar parameter and EW uncertainties was found by adding all the uncertainties in quadrature, as given in the last column of Table 5.

4. RESULTS AND DISCUSSION

4.1. Comparison to Literature Results

In this section, we compare our abundance results to those of different studies from the literature: NRB01, Ishigaki et al. (2010, 2012, 2013), and Frebel et al. (2013). Figure 5 illustrates the overall abundance ([X/H]) pattern found here and in NRB01, with their abundances placed on our solar abundance scale. We also show for comparison a star with similar stellar parameters from the sample of Yong et al. (2013a). This star, HE 1346−0427, has $T_{\rm eff}$/log g/$v_{\rm t}$/[Fe/H] = 6255/3.69/1.40/−3.57, and has an abundance pattern typical for stars of its metallicity (see Figure 43 of Yong et al. 2013a). As can be seen, CD −24°17504 has a similar abundance pattern to this star for elements up to the Fe-peak, apart from C and Al, for which HE 1346−0427 only has upper limits. This confirms that apart from C and the neutron-capture species, CD −24° 17504 also has element abundances typical for stars of its metallicity.

For the elements with atomic number $Z < 29$ in common, the agreement of our results with NRB01 is excellent, apart from Mn. NRB01 measured only the Mn resonance lines, and do not include any systematic correction to the abundances. The ∼0.3 dex discrepancy between their abundance and ours can be entirely explained by the lack of such correction. For the neutron-capture elements, NRB01 provided upper limits for Sr, Y, Ba, and Eu. For all but Sr, we have been able to lower the upper limits for these species by a minimum of 0.40 dex, or a factor of 2.5. Our detections of the 4077 and 4215 Å features yield a larger Sr abundance than found by NRB01 by nearly 0.2 dex. We can reproduce their upper limit using their stellar parameters.

Figure 6 illustrates the comparison to NRB01 another way, along with comparisons to Frebel et al. (2013), Ishigaki et al. (2010, 2012, 2013; placed on our abundance scale, again

Table 6
Element Abundances for CD −24°17504 Based on LTE Stellar Parameters

Species	# lines	logϵ(X)	σ	[X/H]	[X/Fe]	$\sigma/\sqrt{(N)}$
Li I	1	1.99	0.10	…	…	…
1D CH	2	6.12	0.05	−2.31	+1.10	0.04
3D CH[a]	2	5.52	0.05	−2.91	+0.50	0.01
LTE C I[b]	2	5.71	0.05	−2.72	+0.69	0.03
NLTE C I[c]	2	5.45	0.05	−2.98	+0.43	0.03
LTE O I[b]	1	6.12	…	−2.57	+0.84	…
NLTE O I[d]	1	5.70	…	−2.99	+0.42	…
Na I	2	2.60	0.01	−3.64	−0.23	0.01
Mg I	6	4.54	0.05	−3.06	+0.34	0.02
Al I	2	2.44	0.05	−4.02	−0.61	0.04
Si I	1	4.20	0.15	−3.31	+0.10	0.15
Ca I	11	3.18	0.09	−3.16	+0.24	0.03
Sc II	5	−0.05	0.11	−3.20	+0.21	0.05
Ti I	4	2.20	0.05	−2.75	+0.66	0.03
Ti II	16	1.89	0.07	−3.06	+0.35	0.02
Cr I	5	2.23	0.08	−3.41	−0.01	0.04
Mn I	3	2.03	0.03	−3.40	+0.01	0.02
Fe I	113	4.09	0.10	−3.41	…	0.01
Fe II	5	4.09	0.07	−3.41	…	0.03
Co I	4	2.16	0.11	−2.83	+0.57	0.06
Ni I	4	3.16	0.04	−3.06	+0.34	0.03
Zn I	1	2.15	0.15	−2.41	+1.00	0.15
Sr II	2	−1.81	0.02	−4.68	−1.27	0.02
Y II	1	<−1.36	0.18	<−3.57	<−0.16	0.18
Zr II	1	<0.08	0.18	<−2.50	<+0.91	0.18
Ba II	1	<−2.28	0.16	<−4.46	<−1.05	0.16
La II	1	<−1.08	0.17	<−2.18	<+1.23	0.17
Eu II	1	<−1.73	0.16	<−2.25	<+1.16	0.16

Notes.
[a] Applying a −0.6 dex correction to the 1D abundance (Asplund 2005).
[b] Using the EW measures of Fabbian et al. (2009).
[c] Applying a −0.26 dex correction to the LTE abundance as calculated by Fabbian et al. (2009), assuming the $S_H = 1$ scaling of collisions with neutral H atoms.
[d] Applying a −0.45 dex correction to the LTE abundance as calculated by Fabbian et al. (2009), assuming the $S_H = 1$ scaling of collisions with neutral H atoms.

relative to our LTE abundances). Here we distinguish between the results of Ishigaki et al. (2010) from the more recent papers, as the analyses (of the same spectrum) are independent and use very different stellar parameters. In Figure 6, the difference in log ϵ(X), in the sense (This Study—Literature) is shown for each element. Again, the good agreement with NRB01 (black squares) is obvious, apart from the elements already discussed.

Generally, our element abundances are lower than those found by Frebel et al. (2013) and Ishigaki et al. (2012, 2013), and higher than those found by Ishigaki et al. (2010). The difference with Frebel et al. (2013) can largely be explained by the smaller EW measures in this study. The differences with Ishigaki et al. (2010, 2012, 2013) are likely due to the very different atmospheric parameters used in those works (see Figure 3). Adopting the stellar parameters of Ishigaki et al. (2012, 2013) resulted in abundances within 0.1 dex agreement with their values. This is similarly the case when using the Ishigaki et al. (2010) parameters, though abundance discrepencies greater than 0.2 dex remained for Mg and Ti. Interestingly, Ishigaki et al. (2010) present a Ba abundance for CD −24°17504, based on a 1 mÅ EW of the 4554 Å feature (they do not specify it as an upper limit). We can reproduce their abundance, log ϵ(Ba) ≈ −2.8, adopting this EW and their stellar parameters. However, as we cannot see a clear Ba absorption feature of this size in our spectrum, we prefer to determine an upper limit as already described.

4.2. Discussion of Individual Elements

To place the abundances of CD −24°17504 found in this work in context of other known main sequence and turn-off stars of comparable metallicity, we have collected element abundances for stars having stellar paramters within the ranges 5900 K ⩽ $T_{\rm eff}$ ⩽ 6500 K, 3.6 ⩽ log g ⩽ 4.8, and [Fe/H] ⩽ −3.0 from the works of Yong et al. (2013a), Roederer et al. (2014), Cohen et al. (2013), and Aoki et al. (2013). We also include, without any selection criteria, the turn-off star samples of Bonifacio et al. (2009, 2011), Behara et al. (2010), Caffau et al. (2011, 2013a), and Caffau et al. (2013b). In all cases, literature abundances have been placed on the Asplund et al. (2009) solar abundance scale.

4.2.1. Lithium

Figure 7 illustrates spectrum synthesis of the Li I 6707 Å doublet in CD −24°17504. The measured EW of the feature is 18.5 mÅ. The lithium abundance of CD −24°17504 has been subject to previous study (Primas et al. 2000; Meléndez & Ramírez 2004; Aoki et al. 2009; Hosford et al. 2009; Meléndez et al. 2010). The LTE abundance found here, logϵ(Li) = 1.99, is in excellent agreement with that of Primas et al. (2000). As the abundance of Li is sensitive to $T_{\rm eff}$, we see best agreement with literature studies that adopted similar $T_{\rm eff}$ values (that of Primas et al. 2000 is 6300 K). The Keck spectra used in this work were analyzed in Meléndez & Ramírez (2004) and Meléndez et al. (2010). Our measurement of the Li feature is in excellent agreement with theirs, 18.6 mÅ, and the 0.30 dex abundance difference can be attributed to their $T_{\rm eff}$ being ∼225 K hotter than ours.

We determined the NLTE correction to this Li abundance using the grid of Lind et al. (2009) via the "INSPECT" website: (NLTE–LTE) Δlogϵ(Li) = −0.05. This correction is the same regardless of whether we use the LTE or "NLTE" stellar parameters, as the $T_{\rm eff}$ is identical in both cases.

The Li abundance patterns of unevolved extremely metal-poor stars such as CD −24°17504 have been explored to investigate the behavior of the Spite plateau in the low-metallicity regime, and our result does not add anything new to the discussion (e.g., Spite & Spite 1982; Ryan et al. 2001; Meléndez & Ramírez 2004; Bonifacio et al. 2007; Meléndez et al. 2010; Sbordone et al. 2010). We therefore note that our Li abundance for CD −24°17504 is very consistent with those of other stars of similar $T_{\rm eff}$ and [Fe/H] in Sbordone et al. (2010), and refer the reader to that paper for details (see also, e.g., Meléndez et al. 2010).

4.2.2. Carbon

The CH G band is clearly detected in our spectrum of CD −24°17504, as can be seen in Figure 8. The best fit LTE carbon abundance based on the G band is log ϵ(C) = 6.12 ± 0.05, or [C/Fe] = +1.10. Using the "NLTE" stellar parameters, [C/Fe] = +0.83. To our knowledge, this is the first detection of the CH G band in this star. Fabbian et al. (2009) determined a C abundance for CD −24°17504 based on the EW measures of two C I lines in the infrared. They reported LTE

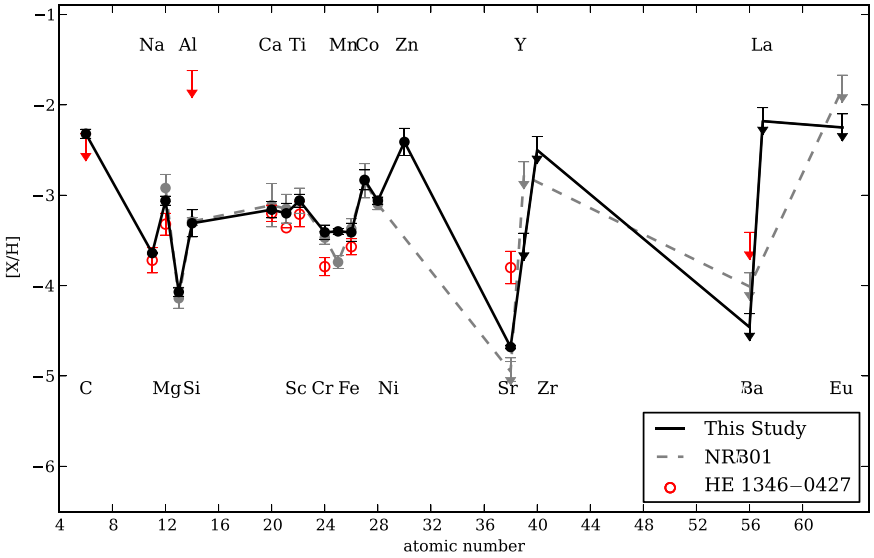

Figure 5. Comparison of element abundances for CD −24°17504 found in this study (LTE; black), compared to that of NRB01 (gray). Upper limits are indicated by arrows; errorbars indicate 1σ line-by-line abundance dispersions. For comparison, we show in red the abundance pattern of HE 1346−0427 from Yong et al. (2013a), which has similar stellar parameters to CD −24°17504 and element abundances typical for stars of its metallicity. See text for more information.

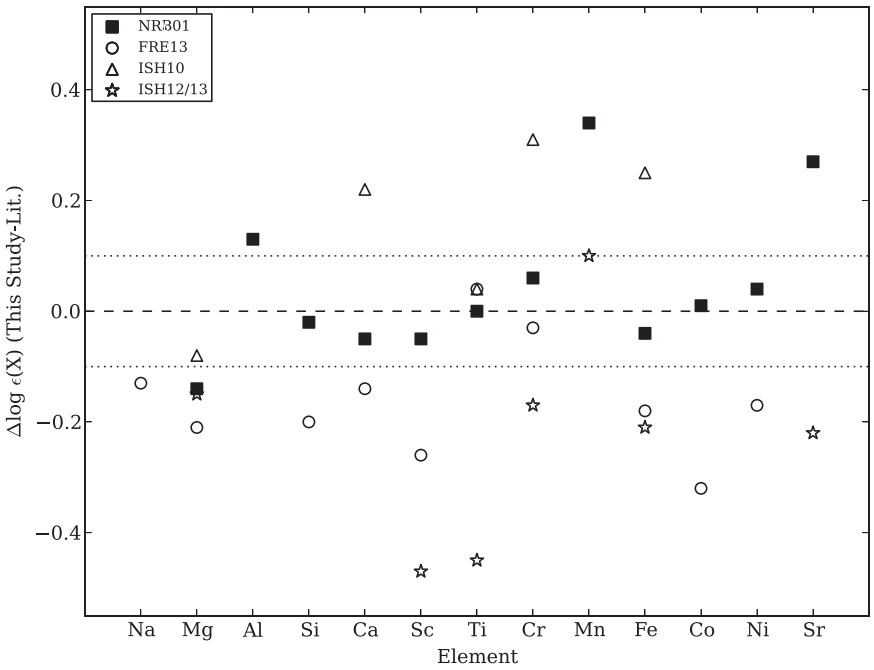

Figure 6. Abundance differences (in the sense this study—Literature) between the present work and three previous studies. Dotted lines indicate Δ log ϵ(X) = ±0.1 to guide the eye. Our results agree with those of NRB01 within 0.1 dex for most elements. See text for more information.

log ϵ(C) = 5.81, or [C/Fe] = +0.59 on the Asplund et al. (2009) solar abundance scale. It is well established in the literature that abundances determined from molecular and atomic C features can greatly differ, due to susceptibility to NLTE and/or 3D effects (Asplund 2005). In particular, NLTE corrections to the C I features used by Fabbian et al. (2009) can be as large as −0.4 dex for a turn-off star of CD −24°17504's metallicity. Likewise, abundances from CH features must be decreased by as much as 0.6 dex to correct for 3D effects (Asplund 2005). To assess whether such corrections can bring our CH abundance in better agreement with the C I result from Fabbian et al. (2009), we have made use of their EW measures to place their abundances on our scale.

First, we confirm their C I abundance using their EWs and stellar parameters (originally from Israelian et al. (2001); see Table 3) with MOOG and a Castelli–Kurucz model atmosphere: log ϵ(C) = 5.80 ± 0.04 (s.d.). C I abundances using our LTE and "NLTE" stellar parameters are shown in Tables 6 and 7. Considering the abundances using the LTE stellar parameters, the C I abundances are ∼0.4 dex lower than the CH carbon abundances. According to Asplund (2005), this is expected if 3D effects are present for CH. However, the C I and CH abundances agree within 0.15 dex when our "NLTE" stellar parameters are used (Table 7).

Also shown in Tables 6 and 7 are the CH and C I abundances corrected for 3D and NLTE effects, respectively. Here, we have

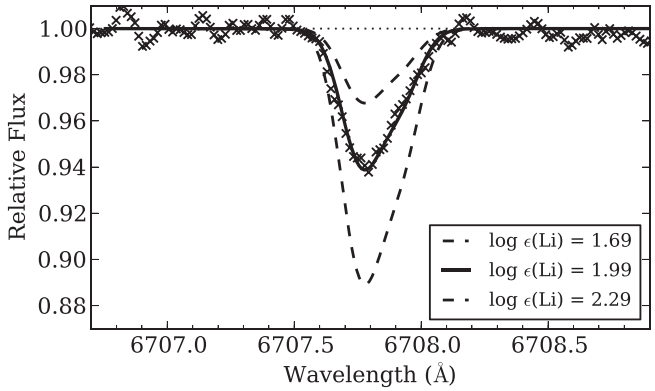

Figure 7. Li 6707 Å doublet in CD −24°17504 (crosses), with the best-fit LTE Li abundance indicated by a solid line. Dashed lines show synthetic spectra with Δ log ϵ(Li) = 0.3 dex around the best value.

applied a −0.6 dex correction to the 1D CH abundances, following Asplund (2005) (see also Bonifacio et al. 2009). For C I abundances, we adopted the NLTE corrections calculated by Fabbian et al. (2009) for CD −24°17504, assuming an $S_H = 1$ scaling factor to collisions with neutral hydrogen atoms (see their Table 3). With these corrections applied, the 3D CH and NLTE C I abundances calculated with the LTE stellar parameters are in good agreement: [C/Fe] ∼ +0.50. However, when using the "NLTE" stellar parameters, there is a ∼0.15 dex disagreement, this time with the C I abundances being larger.

It is possible that it is inappropriate to use the same 3D and NLTE abundance corrections to the abundance results from both the LTE and "NLTE" stellar parameters, as the log g differs by 0.33 dex, and indicate very different evolutionary states for CD −24°17504. It complicates the interpretation of the agreement/disagreement of molecular and atomic carbon features. According to its LTE CH abundance ([C/Fe] = +1.1), it qualifies as a CEMP star according to the definition of Beers & Christlieb (2005) ([C/Fe] > 1) and that set by Aoki et al. (2007) ([C/Fe] > 0.7; the NLTE CH abundance also meets this definition). However, the C I measures of Fabbian et al. (2009) and appropriate 3D corrections indicate [C/Fe] < 1, excluding it from the CEMP population, though it should be stressed the CEMP definitions used in the literature are based on 1D, LTE C abundances.

Figure 9 shows our 1D, LTE [C/Fe] ratio relative to those of other turn-off stars from the literature. Though most of the C abundances for unevolved stars with [Fe/H] $\lesssim$ −3.2 are upper limits, there is a clear indication that the dispersion in [C/Fe] increases with decreasing [Fe/H]. It is also well-established that the fraction of stars that exhibit enhanced [C/Fe] ratios increases with decreasing [Fe/H](Cohen et al. 2005; Lucatello et al. 2006; Carollo et al. 2012; Lee et al. 2013; Yong et al. 2013b; Placco et al. 2014). While CD −24°17504 qualifies as a CEMP star, other stars at comparable metallicity can have much larger enhancements. CEMP stars can be further classified in subcategories, depending on whether or not they exhibit enhancements in other elements (e.g., the neutron-capture species; CEMP-s, CEMP-r/s). As shown in the next sections, CD −24°17504 has normal [X/Fe] ratios for other species and lacks enhancements in neutron-capture elment abundances. Therefore, it can be classified as a CEMP-no ("no" for "normal") star (Beers & Christlieb 2005).

Placco et al. (2014) recently presented a comprehensive compilation of carbon abundances for extremely metal-poor stars in the literature in order to evaluate how the fraction of CEMP stars varies as a function of metallicity. Their analysis included corrections to C abundances as a function of stellar evolutionary state to account for the variation of C due to internal mixing as a star evolves along the giant branch in the HR diagram. As an unevolved star, CD −24°17504 does not need such a correction, and it can be added to the sample of stars with [Fe/H] $\leqslant$ −3 and [C/Fe] $\geqslant$ 1. Based on their literature sample, Placco et al. (2014) found 53/168 = 32% stars meeting this criterion. The addition of CD −24°17504 to this set changes this statistic by only a fraction of a per cent. Considering stars with [Fe/H] $\leqslant$ −3.3, the fraction increases to 41% (35/85) with the inclusion of CD −24°17504.

In summary, the 1D, LTE carbon abundance as measured from the CH G-band in CD −24°17504 indicates that it is a CEMP-no star, relative to comparable measurements (e.g., in 1D, LTE) of other metal-poor stars in the literature.[6] We reiterate, however, that the 3D CH abundance, as well as the abundances of C I lines and abundances determined using the "NLTE" stellar parameters for this star do not fulfill the CEMP star criterion; however, the Beers & Christlieb (2005) and Aoki et al. (2007) definitions would need to be "translated" to be applicable to abundances other than those obtained with 1D/LTE models before arriving at a final conclusion.

4.2.3. Oxygen

Although we do not detect any oxygen absorption features in our spectrum of CD −24°17504, multiple measures of O in CD −24°17504 exist in the literature, and so we include a discussion of them for completeness. Fabbian et al. (2009) report a robust detection of a weak (1.7 mÅ) O I feature at λ7772. Abundances measured from OH features in the near-UV have been reported by Israelian et al. (2001) and Rich & Boesgaard (2009). As for carbon, we place the O measurement by Fabbian et al. (2009) on our abundance scale by using their EW and our stellar parameters (Tables 6 and 7). Using the LTE stellar parameters, we find log ϵ(O) = 6.12 ([O/Fe] = +0.84), which is in good agreement with Fabbian et al. (2009): 6.24. Literature measurements of OH lines result in much larger abundances: Israelian et al. (2001) reported log ϵ(O) = 6.85 ± 0.09, while Rich & Boesgaard (2009) found log ϵ(O) = 6.45 ± 0.15. As both these studies performed spectrum synthesis, we can not reproduce their measures. However, as for carbon, 3D and NLTE effects must be considered for OH and O I abundance measures, respectively. Using the NLTE correction calculated by Fabbian et al. (2009) for CD −24°17504, the O I abundance becomes $[O/H]_{O\,I}$ = −2.99 (LTE parameters) or −2.77 (NLTE parameters). Applying a −0.9 dex correction to the OH abundances (Asplund 2005), $[O/H]_{OH}$ = −2.74 (Israelian et al. 2001), or $[O/H]_{OH}$ = −2.84 (Rich & Boesgaard 2009). Considering the different T_{eff} scales of the different studies, these results are in good agreement.

Few stars in the literature studies we are comparing to in this work (see references in Figure 9) provide O abundances for turn-off stars, so we do not show plots of [O/Fe] versus [Fe/H] here. We refer to the reader to Israelian et al. (2001) and Fabbian et al. (2009) to see the oxygen abundance of CD −24°17504 in the context of other extremely metal-poor

[6] In comparison to G64–12, another star with very similar atmospheric parameters, CD −24°17504 has a ∼0.5 dex higher [C/Fe] ratio, as determined from a 1D, LTE analysis of the CH G band (Barklem et al. 2005).

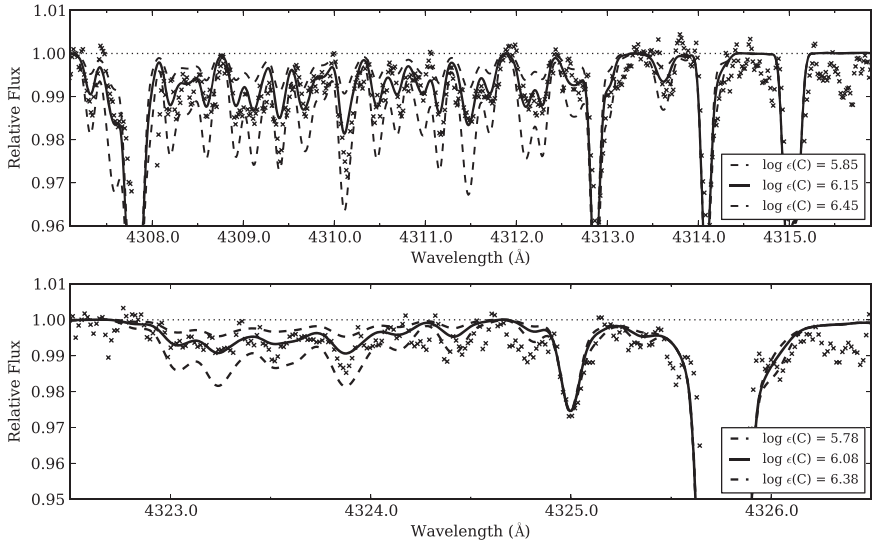

Figure 8. Spectrum synthesis of the G-band CH feature in CD −24°17504. Carbon is definitely detected in this spectrum (points). The best-fit LTE abundance in the two regions is indicated by the bold solid line. Abundances ±0.30 dex are indicated by the dashed lines.

Table 7
Element Abundances for CD −24°17504 Based on "NLTE" Stellar Parameters

Species	# lines	logϵ(X)	σ	[X/H]	[X/Fe]	$\sigma/\sqrt{(N)}$
Li I	1	1.99	0.10	…	…	…
1D CH	2	5.98	0.04	−2.46	+0.83	0.03
3D CH[a]	2	5.38	0.04	−3.05	+0.24	0.03
LTE C I[b]	2	5.83	0.05	−2.60	+0.69	0.03
NLTE C I[c]	2	5.52	0.05	−2.91	+0.38	0.03
LTE O I[b]	1	6.25	…	−2.44	+0.85	…
NLTE O I[d]	1	5.91	…	−2.77	+0.51	…
Na I	2	2.60	0.02	−3.64	−0.35	0.01
Mg I	6	4.53	0.04	−3.07	+0.22	0.02
Al I	2	2.44	0.03	−4.01	−0.72	0.02
Si I	1	4.25	0.15	−3.26	+0.03	0.15
Ca I	11	3.18	0.09	−3.16	+0.13	0.03
Sc II	5	0.05	0.10	−3.10	+0.19	0.04
Ti I	4	2.20	0.05	−2.75	+0.54	0.03
Ti II	16	2.01	0.07	−2.94	+0.35	0.02
Cr I	5	2.24	0.08	−3.40	−0.11	0.04
Mn I	3	2.03	0.03	−3.40	−0.11	0.02
Fe I	113	4.21	0.09	−3.29	…	0.01
Fe II	5	4.21	0.07	−3.29	…	0.03
Co I	4	2.16	0.11	−2.83	+0.46	0.06
Ni I	4	3.17	0.05	−3.04	+0.25	0.03
Zn I	1	2.19	0.15	−2.37	+0.92	0.15
Sr II	2	−1.72	0.03	−4.59	−1.30	0.02
Y II	1	<−1.25	0.18	<−3.46	<−0.17	0.18
Zr II	1	<0.19	0.18	<−2.39	<+0.90	0.18
Ba II	1	<−2.18	0.16	<−4.36	<−1.07	0.16
La II	1	<−0.96	0.17	<−2.06	<+1.23	0.17
Eu II	1	<−1.62	0.16	<−2.14	<+1.15	0.16

Notes. Except where stated, the abundances here do not include additional element-specific NLTE corrections that are qualitatively described in relevant sections in the paper.
[a] Applying a −0.6 dex correction to the 1D abundance (Asplund 2005).
[b] Using the EW measures of Fabbian et al. (2009).
[c] Applying a −0.31 dex correction to the LTE abundance as calculated by Fabbian et al. (2009), assuming the $S_H = 1$ scaling of collisions with neutral H atoms.
[d] Applying a −0.34 dex correction to the LTE abundance as calculated by Fabbian et al. (2009), assuming the $S_H = 1$ scaling of collisions with neutral H atoms.

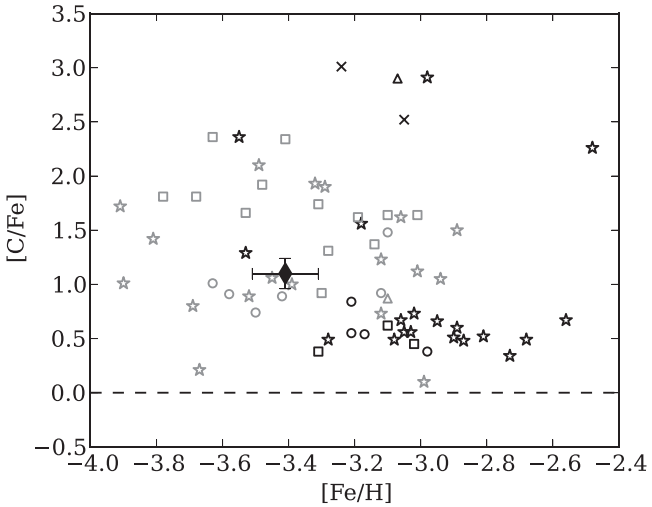

Figure 9. LTE [C/Fe] vs. [Fe/H] for CD −24°17504 (black diamond) and literature stars. Open circles: Roederer et al. (2014; R14), open triangles: Cohen et al. (2013; C13), open squares: Yong et al. (2013a; Y13), crosses: Aoki et al. (2013; A13). The open stars represent results from Bonifacio et al. (2009), Behara et al. (2010), Caffau et al. (2013a, 2013b; Bon). In all cases, black symbols indicate measurements, while gray symbols indicate abundance upper limits.

turn-off stars. Briefly, its [O/Fe] (as measured by both O I and OH species) is in good agreement with general trends shown by other halo stars.

4.2.4. *Light and α Elements*

Figure 10 shows LTE [X/Fe] versus [Fe/H] for the light elements Na and Al, as well as the α-elements for CD−24°17504 and literature stars.[7] As can be seen, CD−24°17504 exhibits [Na/Fe] and [Al/Fe] ratios similar to those of other stars at similar metallicity. We determined

[7] Bonifacio et al. (2011), Caffau et al. (2011, 2013a, 2013b) present abundances of both Ca I and Ca II for their stellar samples. Here we consider only their Ca I abundances, to be consistent with this and other literature studies considered.

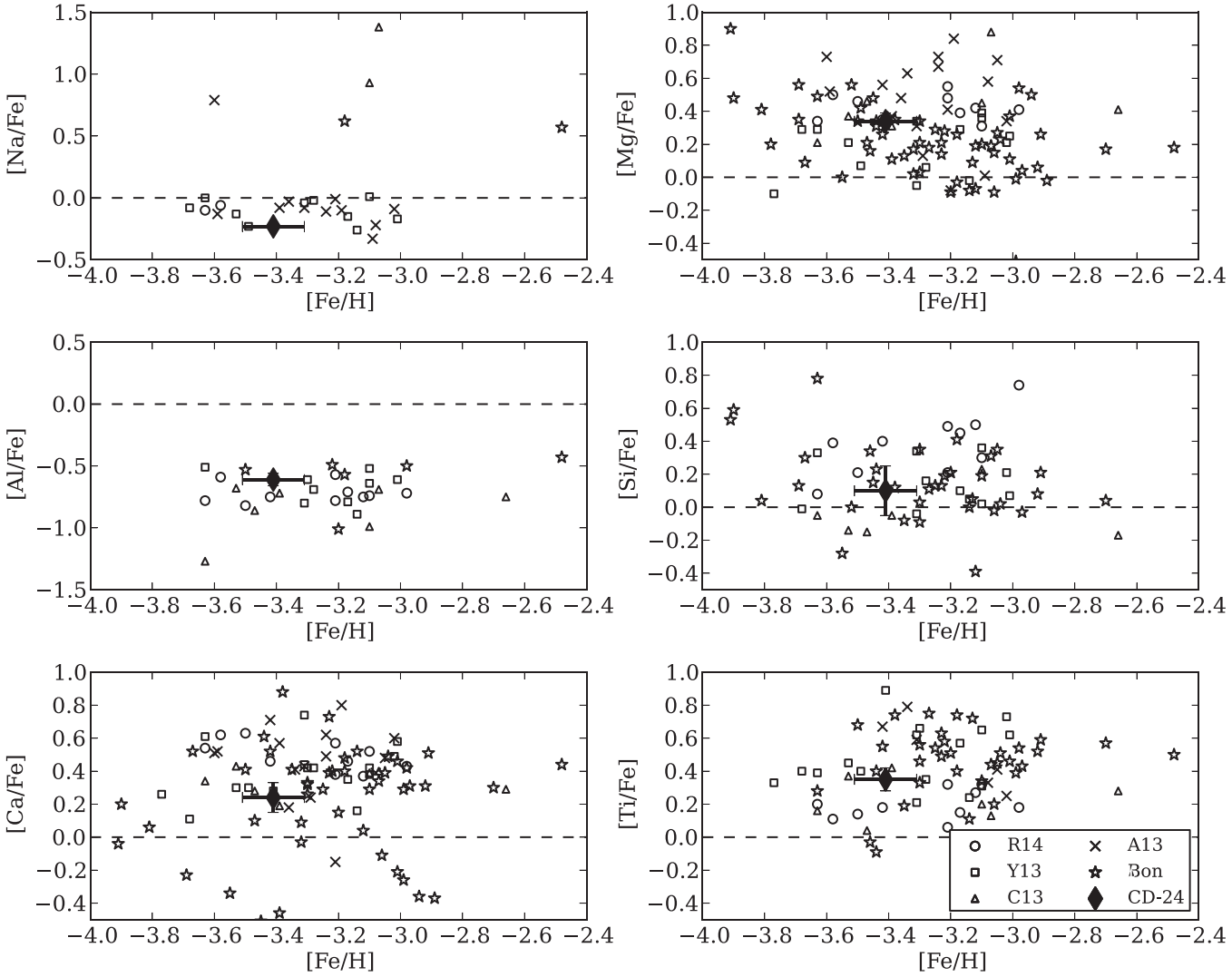

Figure 10. Light and α-element LTE [X/Fe] ratios for CD −24°17504 and literature sample. Symbols same as in Figure 9. We have added 0.65 dex to the Al abundances of Cohen et al. (2013) to place their NLTE abundances on the same scale as the LTE abundances considered here. The Ti abundances shown are those determined from Ti II lines.

NLTE corrections for the two Na I lines considered here using the grid of Lind et al. (2011) in the "INSPECT" website. They are (in the sense NLTE–LTE) −0.07 and −0.06 dex for the 5889 and 5895 Å lines, respectively. Baumueller & Gehren (1997) found NLTE corrections for Al abundances determined from the 3961 Å line to be as large as ∼0.65 dex for stars of similar evolutionary state to CD −24°17504. While their stellar sample did not contain any stars with [Fe/H] < −3, corrections for stars like CD −24°17504 are likely to be at least of the same magnitude. Such corrections would shift the [Al/Fe] ratios shown in Figure 10 to roughly the solar ratio. Solar ratios of [Al/Fe] at low [Fe/H] are much more consistent with predictions of chemical evolution models, as noted by Baumueller & Gehren (1997) and others.

CD −24°17504 also has typical enhanced [α/Fe] ratios ($\langle[\alpha/Fe]\rangle$ = 0.35) for a halo star. For the stars shown in Figure 10, abundance enhancements are typically largest for Mg and Ti, and are less pronounced for Si (though a few stars have [Si/Fe] > +0.5). While many stars have [Ca/Fe] > +0.5, some exhibit sub-solar [Ca/Fe] ratios. Indeed, the number of extremely metal-poor stars that do not show enhanced [α/Fe] ratios has grown in recent years (e.g., Caffau et al. 2013a, 2013b), and their existence indicates a certain degree of inhomogeneity in the chemical enrichment of the early Galaxy, or the sub-halos that built up the Galaxy.

Metal-poor star α-element abundance determinations are also susceptible to NLTE effects. For Mg and Ti, the NLTE corrections are relatively small, ∼+0.1 and −0.05[8] dex, respectively (Gehren et al. 2004; Bergemann 2011). Mashonkina et al. (2007) found NLTE corrections for Ca I lines that varied from +0.10 to +0.29 dex for a warm metal-poor star such as CD −24°17504. Corrections for Si I abundances are even larger: for G64−12, a star with similar parameters to CD −24°17504, Shi et al. (2009) found the NLTE correction for the 3905 Å line abundance to be +0.25 dex. The general impact of these corrections would be to increase the level of α-element enhancement of the stars in Figure 10, but would not necessarily change the interpretation of the data. The

[8] This correction is found for Ti II lines, which are more numerous and reliably measured than Ti I lines in metal-poor star spectra. Consequently, Ti II is more frequently used to determine a star's Ti abundance.

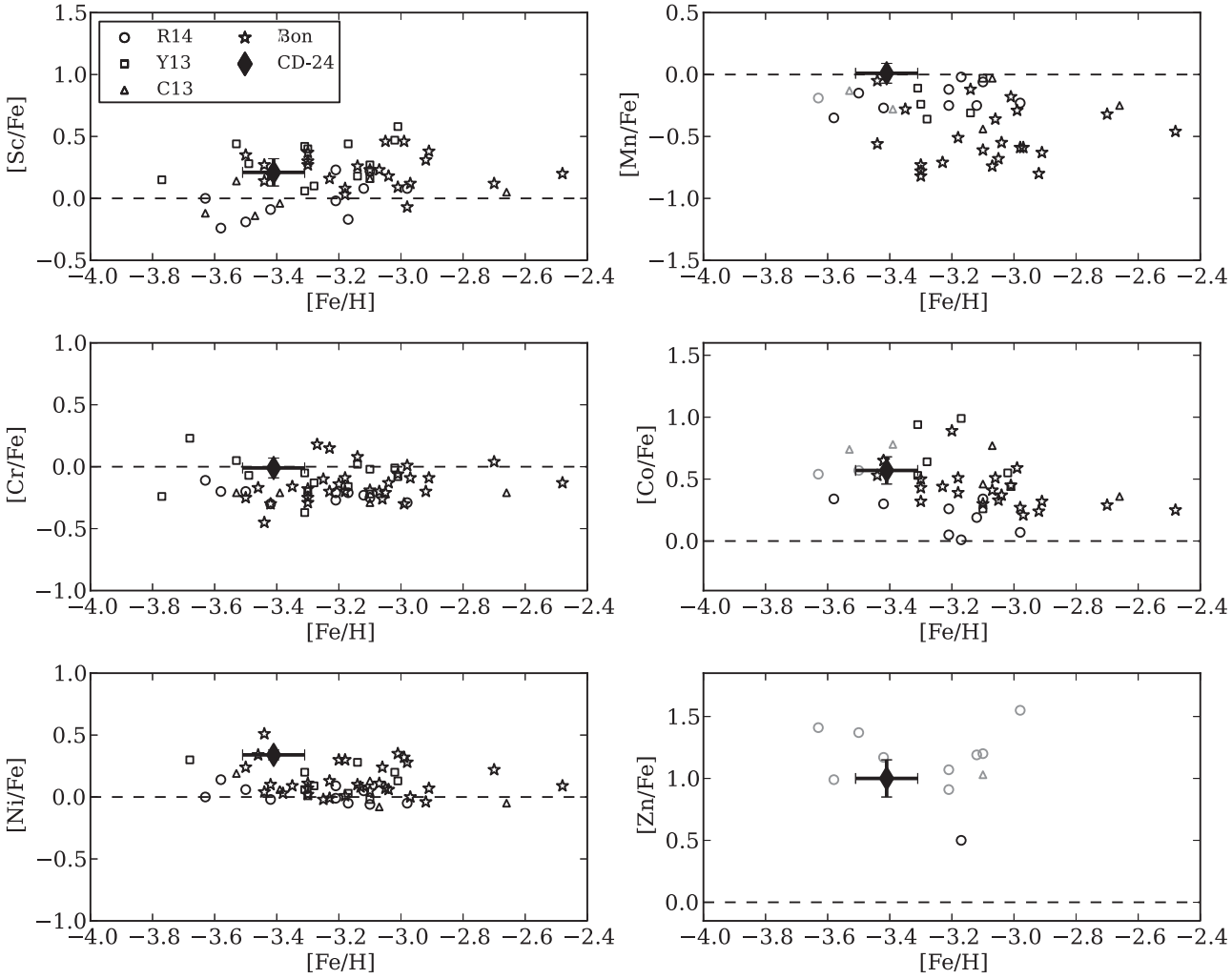

Figure 11. Same as Figure 10 but for scandium and the Fe-peak elements.

[Ca/Fe]-poor stars, for example, would still remain [Ca/Fe]-poor relative to the general halo star population.

4.2.5. Fe-peak Elements

LTE [X/Fe] ratios versus [Fe/H] are shown in Figure 11 for scandium and the Fe-peak elements. Again, the abundance pattern of CD −24°17504 is similar to that of stars of comparable metallicity. The relatively large [Mn/Fe] ratio for CD −24°17504 compared to that of the literature sample can be entirely explained by the 0.3 dex offset applied to the resonance line abundances; such a correction was not performed on the literature results.

The [Ni/Fe] ratio of CD −24°17504, +0.34 dex (LTE), is higher than the typical halo star value that is approximately solar. However, as can be seen in Figure 11, several stars with [Fe/H] < −3 show enhanced [Ni/Fe] ratios. Zn abundances are difficult to determine in metal-poor star spectra, as only a couple weak Zn I lines are present. While these lines can be accurately measured in our spectrum of CD −24°17504, the Zn abundances for most of the metal-poor turn-off stars in the literature are upper limits.

NLTE corrections have been determined for Mn, Cr, and Co. Bergemann & Gehren (2008) found corrections of +0.3 dex are required for the Mn resonance lines, and that is accounted for by our empirically determined correction. Corrections of the order of +0.35–0.40 dex for Cr I lines were found for G64−12 by Bergemann & Cescutti (2010). Given that CD −24° 17504 has similar stellar parameters to G64−12, these corrections are applicable in this case.

Corrections for Co I lines can be as large as +1 dex for cool, evolved metal-poor stars, but in the case of CD −24°17504, the corrections are ∼0.65 dex (Bergemann et al. 2010). Such corrections would place the [Co/Fe] ratios shown in Figure 11 close to [Co/Fe] ∼ 1 and above. As noted by Bergemann et al. (2010), such ratios are at odds with chemical evolution models which use metallicity-dependent supernova yields (e.g., Kobayashi et al. 2006).

4.2.6. Neutron-capture Elements

Of the neutron-capture species that can generally be measured in metal-poor star spectra, only Sr can be detected in even our high S/N spectrum of CD −24°17504. As mentioned in Section 4.1, our *measured* Sr abundance is at slight odds with the upper limit determined by NRB01, being larger by ∼0.2 dex. This difference can be attributed to choice of stellar parameters. Our EWs agree well with theirs: they adopted an upper limit EW of 4 mÅ for both 4077 and 4215 Å Sr II lines, while our bona fide measures are 5.5 and

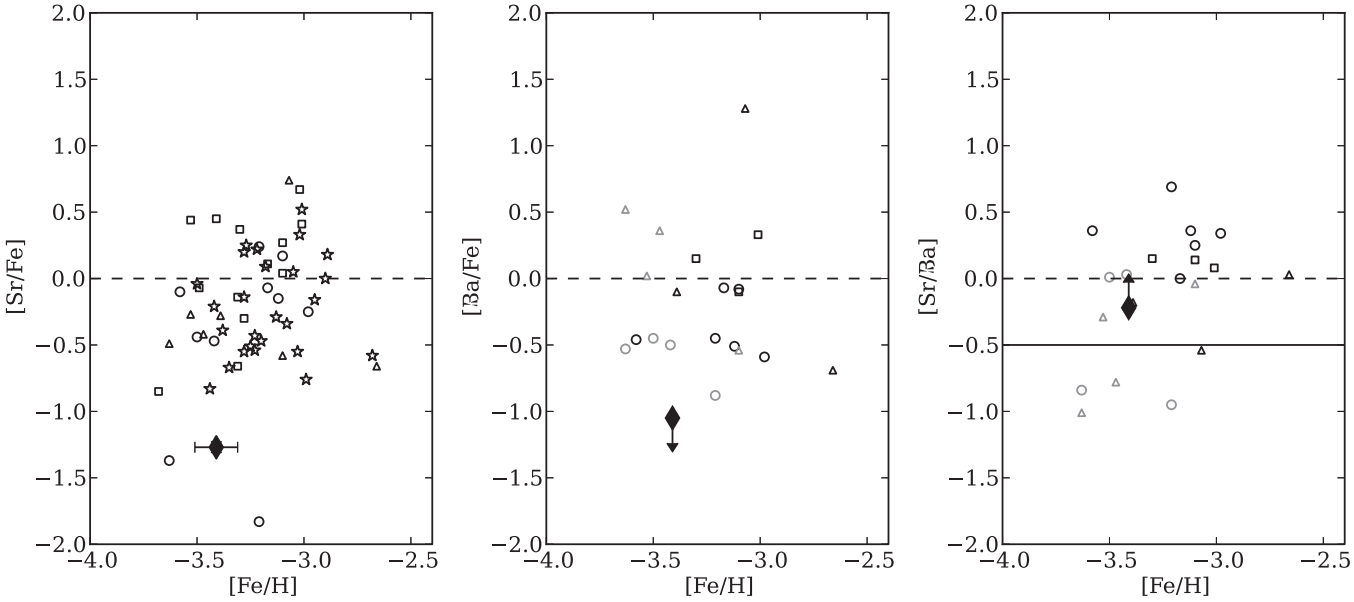

Figure 12. Same as Figure 10 but for the neutron-capture elements Sr and Ba. The right panel shows the ratio of light-to-heavy neutron-capture element abundances, [Sr/Ba], vs. [Fe/H]. The pure *r*-process [Sr/Ba] ratio is indicated by the solid line (Simmerer et al. 2004).

3.1 mÅ, respectively. As can be seen in the left panel of Figure 12, CD −24°17504 exhibits one of the lowest Sr abundances of unevolved metal-poor stars. Although we are considering a relatively narrow range of stellar parameter space (only dwarfs or stars near the MSTO), a >1 dex dispersion in Sr abundances can be observed. This behavior for the neutron-capture elements, in contrast to the ∼0.1 dex dispersion seen for other element groups in the Periodic Table, has been well remarked on in the literature (Burris et al. 2000; Barklem et al. 2005; Sneden et al. 2008; Frebel & Norris 2013).

As described in Section 3.3, upper limits to EWs were determined for neutron-capture species lacking detectable absorption lines in our spectrum. Corresponding abundance upper limits were determined based on these EW upper limits. Our abundance upper limit for barium, [Ba/Fe] < −1.05, is a factor of 2.8 (4.5 dex) lower than the upper limit of NRB01, and is the lowest shown[9] in Figure 12. The last panel of Figure 12 shows [Sr/Ba] versus [Fe/H], which indicates the relative abundances of light to heavy neutron-capture species. Though CD −24°17504 exhibits some of the lowest Sr and Ba abundances, the (lower limit) of their ratio is close to solar and well above the ratio produced by the pure *r*-process. Therefore another source besides the main *r*-process contributed to the Sr abundance in this star, along with that of most of the literature stars also considered here. An analysis of the dispersions in Sr and Ba abundances within a larger, homogeneous sample of unevolved extremely metal-poor stars is the subject of a future paper.

Zr II, Y II, and La II abundances are not commonly included in high resolution spectroscopic studies of metal-poor stars, except in cases where stars show enhancement in neutron-capture element abundances or where the data quality is exceptionally high: their spectroscopic features are generally too weak to measure. They are undetectable even in our high quality data. We include them here because NRB01 determined an upper limit to the Y II abundance of CD −24°17504. For Y, our spectrum allows for a ∼0.8 dex reduction of the lower limit to [Y/Fe] < −0.16. Our upper limits to Zr and La abundances in CD −24°17504 are [Zr/Fe] < +0.91 and [La/Fe] < +1.23, respectively. Our upper limit measure for [Eu/Fe], <+1.16, is 0.4 dex lower than that of NRB01 (<+1.55).

Figure 13 shows [X/Fe] ratios Y, Zr, La, and Eu in CD −24°17504, this time in comparison to the large homogeneous literature sample of Barklem et al. (2005), as most of the literature stars in previous figures lack abundance measurements for these species. We also note that the Barklem et al. (2005) sample is a mixture of evolved and unevolved stars, in contrast to previous figures. As can be seen, the upper limits measures for CD −24°17504 are consistent with the Y, Zr, and La abundances of the literature data, which show varying dispersions of $\lesssim$1 dex for Zr to >2 dex for La and Eu. It is important to repeat the caution of Barklem et al. (2005), however, that given the difficulty of measuring the abundances for these species in most extremely metal-poor stars, the stellar samples in Figure 13 are biased and incomplete. Therefore, it is difficult to draw broad conclusions about the intrinsic abundance patterns and dispersions for these elements in the context chemical evolution.

More firm interpretations can be made from the Sr and Ba abundances of extremely metal-poor stars, however, as those samples are much more complete and unbiased. With [Sr/H] ≈ −4.7 and [Ba/H] $\leqslant$ −4.5, CD −24°17504 is among the Milky Way halo stars with the lowest neutron-capture element enhancements (e.g., Figure 1 of Roederer 2013 and Figure 7 of Frebel et al. 2014). Such low levels of neuton-capture abundances are common in stars in ultra-faint dwarf galaxies (e.g., Frebel et al. 2014 and references therein). These low-mass systems are thought to be the remaining analogs of the "proto-galaxies" that were the early building blocks of large galaxies such as the Milky Way, as only one or two stellar generations contributed to their chemical enrichment before star formation was quenched. Therefore, if low levels of neutron-capture enrichment is a signature of these primitive

[9] We note that other stars not considered here can exhibit comparably low [Ba/Fe] abundances. See, e.g., Figure 7 in Frebel et al. (2014) for a recent comprehensive literature compilation.

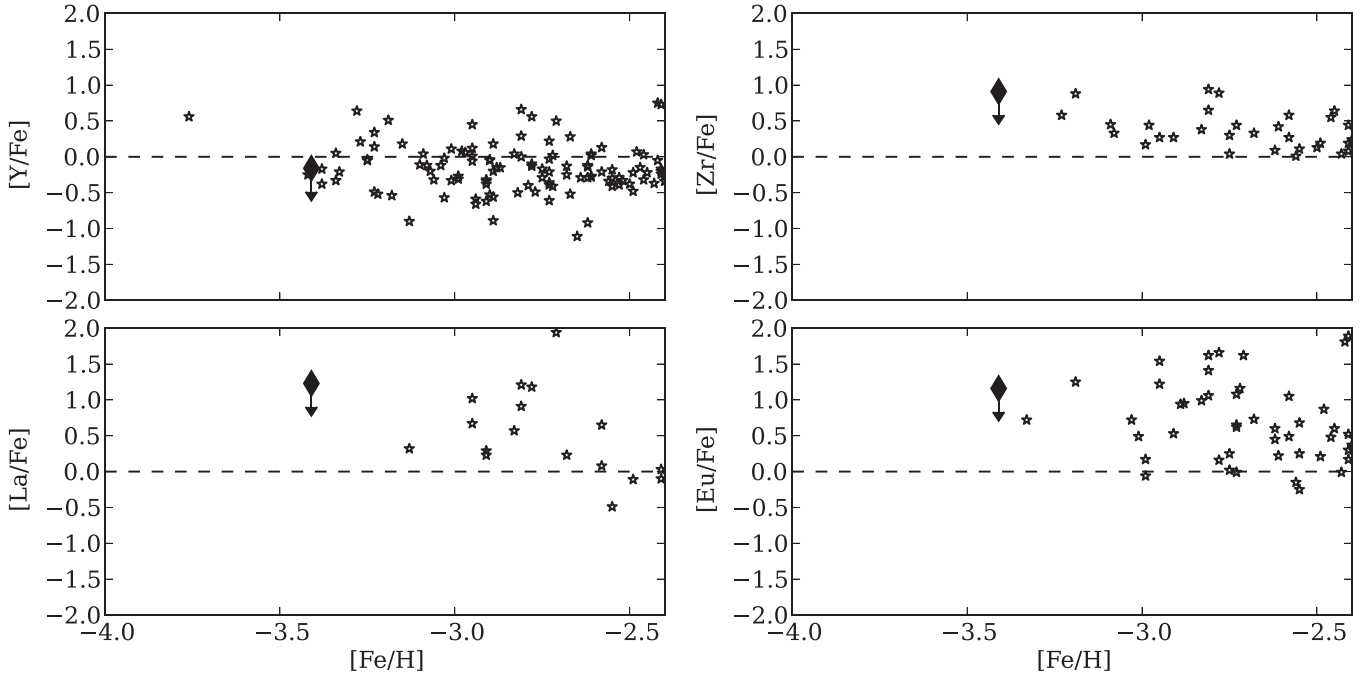

Figure 13. The LTE upper limit [X/Fe] ratios for the elements Y, Zr, La and Eu in CD −24°17504 (filled diamonds), this time in comparison to the sample of Barklem et al. (2005) (stars).

systems, then the Milky Way halo stars with low Sr and Ba abundances such as CD −24°17504 may have originated in such systems (Frebel & Norris 2015). Given the high proper motion of CD −24°17504, its kinematics may also provide clues to its origin.

Such statements are generally made regarding LTE neutron-capture element abundances, however. Bergemann et al. (2012a) found (NLTE–LTE) abundance corrections for the Sr II 4077 feature of −0.05 to 0 dex for unevolved stars at [Fe/H] = −3, but this correction can reach +0.15 at lower metallicities. Andrievsky et al. (2011) found NLTE corrections depended upon a star's Sr abundance as well as its stellar parameters. For a star with CD −24°17504's $T_{\rm eff}$, [Fe/H], and Sr abundance, they found a correction of ∼+0.25 dex (their Figure 7). Similarly, Andrievsky et al. (2009) found NLTE corrections to Ba abundances measured from the Ba II 4554 line also depend on effective temperature and Ba abundance (see also Mashonkina et al. 1999). They did not provide corrections for [Ba/H] < −3 in their work, but for turnoff stars with similar parameters to CD −24°17504 they calculated NLTE corrections ranging from +0.07 to +0.37 dex. For the remaining neutron-capture element most commonly studied in metal-poor stars, Eu, NLTE corrections are ∼+0.05–0.10 dex for unevolved stars (Mashonkina et al. 2003).

4.3. Effects of Internal Diffusion Processes

The surface abundance of a star can differ from its primordial chemical composition due to internal diffusion processes throughout its lifetime, such as convection, gravitational settling, and radiative acceleration (e.g., Richard et al. 2002b; Korn et al. 2007, 2009). Richard et al. (2002a) pointed to CD −24°17504 specifically as an extremely metal-poor turnoff star whose observed abundance pattern may differ greatly from its initial composition. Indeed, the ∼500 K range in $T_{\rm eff}$ found for CD −24°17504 by different studies (Figure 3, Table 3) indicate very different evolutionary states for CD −24°17504, so it is difficult to quantify the magnitude of its abundance variations. However, looking at Figures 10 and 11 of Richard et al. (2002a), one can get a sense of how large the abundance variations might be for specific elements, spanning the range of $T_{\rm eff}$ values measured for CD −24°17504.

For example, depending on its evolutionary state, the measured Fe abundance of CD −24°17504 may be as much as ∼0.3 dex underabundant to ∼0.9 dex overabundant relative to its intitial [Fe/H]. Ca may also be under- or overabundant by as much as ∼0.5 dex. Carbon and oxygen can be depleted by nearly 2 dex, while species such as Na, Mg, Cr and Mn can be 0.2 to 0.4 dex below their initial values. Alternatively, Al, Si and Ni can be 0.3–0.4 dex enhanced.

Based on our abundance analysis (Tables 6, 7), the [X/Fe] ratios of Na, Cr, Mn, and Ni are consistent with the model predictions of Richard et al. (2002a), but the [Al/Fe] < 0 and [Si/Fe] ∼ 0 ratios disagree. In order to better compare the abundance pattern of CD −24°17504 to models that include diffusion effects, it is necessary to more tightly constrain its evolutionary status by decreasing the dispersion in stellar parameters found by different studies using different methods. For now, the discussion in this work and others of how the abundance pattern of CD −24°17504 compares to other halo stars (e.g., Figures 9–13) should be viewed cautiously until the effects of internal diffusion are better understood.

5. SUMMARY

We have presented a comprehensive element abundance analysis of the canonical metal-poor turn-off star CD −24°17504 based on high-resolution, high S/N archival spectra. Though comparable in resolution to other studies of CD −24°17504, the extremely high S/N (∼400 in some places) of our data allow for more robust equivalent width measurements and a factor of >3 improvement in the lower limits to

some element abundances. Our analysis began with a classical spectroscopic determination of stellar parameters with the addition of an empirical correction to effective temperature. We also performed an "NLTE" parameter determination following the method of Ruchti et al. (2013). LTE and "NLTE" abundances were then determined for 20 other species using both EWs and spectrum synthesis techniques. Our resulting stellar parameters, metallicity, and element abundances agree well with those of other studies, including that of NRB01. In particular, we have found the following:

1. CD −24°17504 has [Fe/H] = −3.41 and [Fe/H] = −3.29, assuming LTE and NLTE, respectively. This value is in good agreement with studies in the literature. Its [X/Fe] ratios for the light, α and Fe-peak elements are comparable to those of other halo stars at similar metallicity.
2. Based on a clear detection of the CH G-band feature in our spectrum of CD −24°17504, we have measured it to have [C/Fe] = +1.10. As it lacks enhancements in any neutron-capture element abundances, it can therefore be classified as a CEMP-no star according to the definition of Beers & Christlieb (2005). It is among the ∼40% of stars with [Fe/H] $\leqslant$ −3.3 that have [C/Fe] $\geqslant$ 1 (Placco et al. 2014). However, the C abundance as measured by infrared C I lines (Fabbian et al. 2009) is ∼0.3 dex lower, serving as a reminder that 3D and NLTE effects should not be disregarded and may change our current understanding of the behavior of [C/Fe] versus [Fe/H] for extremely metal-poor stars, which generally are based on 1D, LTE measures of CH features in stellar spectra.
3. We have compared literature oxygen abundances for CD −24°17504 as measured by near-ultraviolet OH features and the O I triplet. Making appropriate 3D and NLTE corrections brings these O abundances into good agreement, and indicates that CD −24°17504 has [O/Fe] ∼ +0.5.
4. We have decreased the upper limit abundance estimates for elements Ba, Y, and Eu by 0.4–0.8 dex compared to NRB01, and also provide an upper limit measure for Zr and La. The upper limits for Y, Zr, La, and Eu are comparable to values found in other metal-poor stars in the literature, though data remains sparse for some of these elements.
5. CD −24°17504 has (LTE) [Sr/H] ∼ −4.7 and [Ba/H] $\lesssim$ −4.5, which are among the lowest Sr and Ba abundances exhibited by extremely metal-poor stars in the Milky Way halo. Such low neutron-capture element abundances are more characteristic of stars in ultra-faint dwarf galaxies, and may therefore indicate that CD −24°17504 originated in a high-redshift analog of such a system.
6. We briefly review the abundance pattern of CD −24°17504 relative to the predicted abundance variations caused by internal diffusion processes in a metal-poor turn-off star. The [X/Fe] ratios of some elements are consistent with model predictions, but others disagree. The location of CD −24°17504 on the Hertzsprung–Russell diagram must be more tightly constrained before the magnitude of possible abundance variations can be determined.

The authors warmly thank A. R. Casey for the development of SMH and for making available scripts used to combine the archival data, as well as for discussions about and his assistance with checking the quality of the combined spectrum. We are grateful to the referee for comments that improved the presentation of these results. This research has made use of data obtained from the ESO Science Archive Facility and the Keck Observatory Archive. We also acknowledge use of the SIMBAD database, operated at CDS, Strasbourg, France and of NASA's Astrophysics Data System Bibliographic Services. This work also includes data obtained from the INSPECT database (v1.0). A.F. acknowledges support from NSF grant AST-1255160.

Facilities: Keck:I (HIRES), VLT:Kueyen (UVES)

REFERENCES

Andrievsky, S. M., Spite, F., Korotin, S. A., et al. 2011, A&A, 530, A105
Andrievsky, S. M., Spite, M., Korotin, S. A., et al. 2009, A&A, 494, 1083
Aoki, W., Barklem, P. S., Beers, T. C., et al. 2009, ApJ, 698, 1803
Aoki, W., Beers, T. C., Christlieb, N., et al. 2007, ApJ, 655, 492
Aoki, W., Beers, T. C., Lee, Y. S., et al. 2013, AJ, 145, 13
Arnone, E., Ryan, S. G., Argast, D., Norris, J. E., & Beers, T. C. 2005, A&A, 430, 507
Asplund, M. 2005, ARA&A, 43, 481
Asplund, M., Grevesse, N., Sauval, A. J., & Scott, P. 2009, ARA&A, 47, 481
Barklem, P. S., Christlieb, N., Beers, T. C., et al. 2005, A&A, 439, 129
Baumueller, D., & Gehren, T. 1997, A&A, 325, 1088
Beers, T. C., & Christlieb, N. 2005, ARA&A, 43, 531
Beers, T. C., Preston, G. W., & Shectman, S. A. 1992, AJ, 103, 1987
Behara, N. T., Bonifacio, P., Ludwig, H.-G., et al. 2010, A&A, 513, A72
Bergemann, M. 2011, MNRAS, 413, 2184
Bergemann, M., & Cescutti, G. 2010, A&A, 522, A9
Bergemann, M., & Gehren, T. 2008, A&A, 492, 823
Bergemann, M., Hansen, C. J., Bautista, M., & Ruchti, G. 2012a, A&A, 546, A90
Bergemann, M., Lind, K., Collet, R., Magic, Z., & Asplund, M. 2012b, MNRAS, 427, 27
Bergemann, M., Pickering, J. C., & Gehren, T. 2010, MNRAS, 401, 1334
Bihain, G., Israelian, G., Rebolo, R., Bonifacio, P., & Molaro, P. 2004, A&A, 423, 777
Bonifacio, P., Caffau, E., François, P., et al. 2011, AN, 332, 251
Bonifacio, P., Molaro, P., Sivarani, T., et al. 2007, A&A, 462, 851
Bonifacio, P., Spite, M., Cayrel, R., et al. 2009, A&A, 501, 519
Burris, D. L., Pilachowski, C. A., Armandroff, T. E., et al. 2000, ApJ, 544, 302
Caffau, E., Bonifacio, P., François, P., et al. 2011, A&A, 534, A4
Caffau, E., Bonifacio, P., François, P., et al. 2013a, A&A, 560, A15
Caffau, E., Bonifacio, P., Sbordone, L., et al. 2013b, A&A, 560, A71
Carollo, D., Beers, T. C., Bovy, J., et al. 2012, ApJ, 744, 195
Casey, A. R. 2014, arXiv: 1405.5968
Castelli, F., & Kurucz, R. L. 2004, arXiv: astro-ph/0405087
Cayrel, R. 1988, in IAU Symp. 132, The Impact of Very High S/N Spectroscopy on Stellar Physics, ed. G. Cayrel de Strobel & M. Spite (Dordrecht: Kluwer), 345
Cayrel, R., Depagne, E., Spite, M., et al. 2004, A&A, 416, 1117
Christlieb, N., Schörck, T., Frebel, A., et al. 2008, A&A, 484, 721
Cohen, J. G., Christlieb, N., Thompson, I., et al. 2013, ApJ, 778, 56
Cohen, J. G., Shectman, S., Thompson, I., et al. 2005, ApJL, 633, L109
Fabbian, D., Nissen, P. E., Asplund, M., Pettini, M., & Akerman, C. 2009, A&A, 500, 1143
Frebel, A., Casey, A. R., Jacobson, H. R., & Yu, Q. 2013, ApJ, 769, 57
Frebel, A., & Norris, J. E. 2013, in Metal-Poor Stars and the Chemical Enrichment of the Universe, ed. T. D. Oswalt & G. Gilmore (Berlin: Springer)
Frebel, A., & Norris, J. E. 2015, arXiv: 1501.06921
Frebel, A., Simon, J. D., & Kirby, E. N. 2014, ApJ, 786, 74
Gehren, T., Liang, Y. C., Shi, J. R., Zhang, H. W., & Zhao, G. 2004, A&A, 413, 1045
Hosford, A., Ryan, S. G., García Pérez, A. E., Norris, J. E., & Olive, K. A. 2009, A&A, 493, 601
Ishigaki, M., Chiba, M., & Aoki, W. 2010, PASJ, 62, 143
Ishigaki, M. N., Aoki, W., & Chiba, M. 2013, ApJ, 771, 67
Ishigaki, M. N., Chiba, M., & Aoki, W. 2012, ApJ, 753, 64
Israelian, G., Rebolo, R., García López, R. J., et al. 2001, ApJ, 551, 833
Kim, Y.-C., Demarque, P., Yi, S. K., & Alexander, D. R. 2002, ApJS, 143, 499

Kobayashi, C., Umeda, H., Nomoto, K., Tominaga, N., & Ohkubo, T. 2006, ApJ, 653, 1145
Korn, A. J., Grundahl, F., Richard, O., et al. 2007, ApJ, 671, 402
Korn, A. J., Richard, O., Mashonkina, L., et al. 2009, ApJ, 698, 410
Lai, D. K., Bolte, M., Johnson, J. A., et al. 2008, ApJ, 681, 1524
Lee, Y. S., Beers, T. C., Masseron, T., et al. 2013, AJ, 146, 132
Lind, K., Asplund, M., & Barklem, P. S. 2009, A&A, 503, 541
Lind, K., Asplund, M., Barklem, P. S., & Belyaev, A. K. 2011, A&A, 528, A103
Lind, K., Bergemann, M., & Asplund, M. 2012, MNRAS, 427, 50
Lucatello, S., Beers, T. C., Christlieb, N., et al. 2006, ApJL, 652, L37
Luyten, W. J. 1980, NLTT Catalogue (Minneapolis, MN: Univ. Minnesota Press)
Mashonkina, L., Gehren, T., & Bikmaev, I. 1999, A&A, 343, 519
Mashonkina, L., Gehren, T., Travaglio, C., & Borkova, T. 2003, A&A, 397, 275
Mashonkina, L., Korn, A. J., & Przybilla, N. 2007, A&A, 461, 261
Meléndez, J., Casagrande, L., Ramírez, I., Asplund, M., & Schuster, W. J. 2010, A&A, 515, L3
Meléndez, J., & Ramírez, I. 2004, ApJL, 615, L33
Nissen, P. E., Akerman, C., Asplund, M., et al. 2007, A&A, 469, 319
Norris, J. E., Bessell, M. S., Yong, D., et al. 2013, ApJ, 762, 25
Norris, J. E., Ryan, S. G., & Beers, T. C. 2001, ApJ, 561, 1034
Placco, V. M., Frebel, A., Beers, T. C., & Stancliffe, R. J. 2014, ApJ, 797, 21
Primas, F., Molaro, P., Bonifacio, P., & Hill, V. 2000, A&A, 362, 666
Rich, J. A., & Boesgaard, A. M. 2009, ApJ, 701, 1519
Richard, O., Michaud, G., & Richer, J. 2002a, ApJ, 580, 1100
Richard, O., Michaud, G., Richer, J., et al. 2002b, ApJ, 568, 979
Roederer, I. U. 2013, AJ, 145, 26
Roederer, I. U., Preston, G. W., Thompson, I. B., et al. 2014, AJ, 147, 136
Roederer, I. U., Sneden, C., Thompson, I. B., Preston, G. W., & Shectman, S. A. 2010, ApJ, 711, 573
Ruchti, G. R., Bergemann, M., Serenelli, A., Casagrande, L., & Lind, K. 2013, MNRAS, 429, 126
Ryan, S. G. 1989, AJ, 98, 1693
Ryan, S. G., Kajino, T., Beers, T. C., et al. 2001, ApJ, 549, 55
Ryan, S. G., & Norris, J. E. 1991, AJ, 101, 1835
Ryan, S. G., Norris, J. E., & Bessell, M. S. 1991, AJ, 102, 303
Sbordone, L., Bonifacio, P., Caffau, E., et al. 2010, A&A, 522, A26
Shi, J. R., Gehren, T., Mashonkina, L., & Zhao, G. 2009, A&A, 503, 533
Simmerer, J., Sneden, C., Cowan, J. J., et al. 2004, ApJ, 617, 1091
Sneden, C. A. 1973, PhD thesis, Univ. Texas, Austin
Sneden, C., Cowan, J. J., & Gallino, R. 2008, ARA&A, 46, 241
Sobeck, J. S., Kraft, R. P., Sneden, C., et al. 2011, AJ, 141, 175
Spite, F., & Spite, M. 1982, A&A, 115, 357
Spite, M., Francois, P., Nissen, P. E., & Spite, F. 1996, A&A, 307, 172
Thévenin, F., & Idiart, T. P. 1999, ApJ, 521, 753
Thome, J. M. 1892, Cordoba Durchmusterung, Vol. 16 (Buenos Aires: Coni)
Yong, D., Norris, J. E., Bessell, M. S., et al. 2013a, ApJ, 762, 26
Yong, D., Norris, J. E., Bessell, M. S., et al. 2013b, ApJ, 762, 27